Report
P-20-16
August 2020

Bentonite erosion project

Preliminary study for the numerical simulation of bentonite erosion

Arnau Pont
Emilie Coene
Andrés Idiart

SVENSK KÄRNBRÄNSLEHANTERING AB

SWEDISH NUCLEAR FUEL
AND WASTE MANAGEMENT CO

Box 3091, SE-169 03 Solna
Phone +46 8 459 84 00
skb.se

SVENSK KÄRNBRÄNSLEHANTERING

ISSN 1651-4416
SKB P-20-16
ID 1898092

August 2020

Bentonite erosion project

Preliminary study for the numerical simulation of bentonite erosion

Arnau Pont, Emilie Coene, Andrés Idiart
Amphos 21 Consulting S.L.

Summary

In this work, the model for quantifying bentonite expansion and erosion developed by Neretnieks et al. (2009), Liu et al. (2009) and Moreno et al. (2010) is revisited and a series of improvements are proposed. The final goal consists in providing a complete computational framework that considers all relevant features under realistic repository conditions. In the present work, focus is made on understanding, modelling and quantifying the expansion or extrusion of bentonite within intersecting fractures, which is the main objective. One of the key features under consideration is the effect of wall friction on limiting bentonite expansion when the concentration of the contacting low salinity solution drops to the Critical Coagulation Concentration (CCC). This effect is deeply related to bentonite swelling pressure and shear strength and is thought to have a direct side-effect on the resistance to erosion. The proposed modelling features are tested by simulating several laboratory tests with different fracture apertures.

A second objective is to preliminarily study bentonite mass loss due to erosion when exposed to seeping water through a fracture. The interaction between seeping water and a dilute sol is an aspect that cannot be fully captured by the Darcy equations, as used in existing models to describe water flow in a fracture. For this reason, special attention is paid to the flow equations to provide a qualitative estimation of bentonite erosion without resorting to empirical approaches.

The models developed in this work are implemented in COMSOL Multiphysics and tested against existing experimental data from simplified small-scale laboratory tests of the expansion of bentonite into artificial fractures with or without a forced flow. In cases with flow, a preliminary analysis of the eroded mass is attempted. The modelling results show the necessity of extending the Darcy flow equations to a Brinkman model in order to capture the viscous interaction between sol and seeping water, as well as the importance of swelling pressure in the balance between bentonite expansion and erosion.

The tests under consideration had durations ranging from 19 to 30 days. Such a short temporal scope allows considering a constant bentonite chemical composition. However, the bentonite porewater sodium concentration might be diluted under repository conditions below CCC by the action of glacial groundwater after some years. This could entail a serious threat for the integrity of the bentonite barrier. For this reason, a second part of this study focuses on long-term solute transport in a system comprised by a bentonite buffer intersected by a fracture with seeping water.

Finally, the leaching of solute from the bentonite buffer under the action of glacial water in the KBS-3V repository concept is analysed. Although the influence of chemical reactions between bentonite and glacial water involved in this process is not assessed, two transport models are evaluated in order to estimate the time span before reaching the Critical Coagulation Concentration (CCC), the ionic concentration of the groundwater in the fracture below which the integrity of the bentonite buffer would be seriously endangered by erosion.

Sammanfattning

I den här studien den modell som kvantifierar expansion och erosion, som var utvecklad av Neretnieks et al. (2009), Liu et al. (2009) och Moreno et al. (2010) omprövats och ett antal förbättringar föreslås. The slutliga målet är att ta fram fullständigt beräkningsverktyg som hanterar alla relevanta processer och funktioner under förvarförhållanden. I detta arbete har fokus dock varit på att förstå, modellera och kvantifiera expansion, eller extrudering, av bentonit in i sprickor som är i kontakt med deponeringshålet. En av nyckelkomponenterna som studerats är effekt av väggfriktion på expansionen när den omgivande lösningen har en salthalt som sjunker ner mor den kritiska koaguleringskoncentrationen (CCC). Denna effekt är starkt relaterad till svälltrycket och skjuvhållfastheten och skulle kunna ha sidoeffekten att den begränsar expansionen. De föreslagna modellkomponenterna testades genom att simulera flera laboratorieförsök med olika sprickaperturer.

Ett andra mål var att göra en preliminär studie an massförlust av bentonit genom erosion under förhållanden med strömmande vatten i en spricka. Interaktionen mellan strömmande vatten och en utspädd sol kan inte helt beskrivas med Darcys ekvationer, vilka används i befintliga modeller för att beskriva vattenflöde i sprickor. Därför har särskild hänsyn tagit till flödesekvationerna för att kunna göra en kvalitativ uppskattning av bentoniterosion utan att behöva använda empiriska samband.

De modeller som har utvecklas I den här studien har implementerat i COMSOL Multiphysics och testats mot tillgänglika experimentella data från förenklade småskaliga laboratorietester, vilka studerar expansion av bentonit in i konstgjorda sprickor, med eller utan vattenflöde. I fall med flöde har en preliminär analys av massförlust gjorts. Modellresultaten visar att det är nödvändigt att utöka Darcys flödesekvationer till en Brinkmanmodell för att fånga den viskösa interaktionen mellan en sol och det flödande vattnet, samt betydelsen av svälltrycket i balansen mellan bentonitens expansion och erosion.

De tester som har studerats hade en varaktighet på mellan 19 och 30 dagar. Så korta tider gör det möjligt att anta att bentoniten har en konstant kemisk sammansättning. Emellertid är det tänkbart att natriumkoncentrationen i bentonitens porvatten bli utspädd till nivåer under CCC efter en tid i förvaret till följd av inträngning av utspädda vatten. Detta skulle kunna innebära ett hot mot bentonitbarriärens integritet. Därför fokuserar den andra delen av den här studien på långsiktigt transport av lösta specier i ett system med en bentonitbarriär som genomkorsas av en vattenförand spricka.

Slutligen analyseras utlakningen av lösta ämnen från bentonitbarriären i ett KBS-3 förvar under förhållanden med utspädda grundvatten. Två olika transportmodeller utvärderades för att uppskatta tidspannet innan den kritiska koaguleringskoncentrationen (CCC) nås. Detta är den koncentration i grundvattnet när bentonitens integritet kan påverkas av erosion. Modellerna tar dock inte hänsyn till kemiska reaktioner mellan bentoniten och grundvattnet.

Contents

1 Introduction

1.1 Background

In recent years, the mechanisms of bentonite erosion have been intensively investigated to better understand their potential impacts on the long-term integrity of the compacted bentonite buffer in the KBS-3V concept over the long term. An EU integrated project (named BELBaR project) was running between 2012 and 2016 and several experiments and modelling approaches were conducted and developed. As a result, the erosion models previously used by SKB and Posiva in the initial long-term safety assessments for the final repositories for spent nuclear fuel were further developed and refined. The refined model can be transformed into a relatively simple expression that can be used for quantitative assessments (Neretnieks et al. 2017). However, there are large uncertainties regarding some of the expansion (or extrusion) and erosion mechanisms, such as gravity, flocculation and friction, which still need to be properly integrated in a computational model.

In this sense, the current POSKBAR project aims at quantifying the mass loss of bentonite from the buffer due to erosion triggered by low salinity groundwater below the Critical Coagulation Concentration (CCC) by two means: experimentally with simplified laboratory tests (Alonso et al. 2019), and numerically with a computational model that overcomes the limitations of the existing modelling approaches.

1.2 State of the art modelling approaches

The model developed by Neretnieks and coworkers (Neretnieks et al. 2009, Liu et al. 2009, Moreno et al. 2010), from now on referred to as Neretnieks' model, is the first phenomenological approach to describe bentonite expansion and erosion. It consists in the coupling of a set of three equations corresponding to sodium cation transport, smectite expansion and water flow in a fracture, with special focus on the smectite diffusion equation. The early work by Ahn et al. (1999) and Kanno et al. (2001), as well as Borrelli and Ahn (2008), directly based the diffusivity of smectite on a precomputed correlation for bentonite swelling pressure. In turn, Neretnieks' model is based on a mechanistic description of the nanoscale forces driving bentonite motion. In that model, the swelling capacity is expressed as a balance between the repulsive Diffuse Double Layer (DDL) force and the attractive van der Waals force. In turn, these forces show an explicit dependence on the two concentration variables of the model – i.e. sodium cation concentration and smectite volume fraction –, for which it can in principle be applied to a wide range of scenarios.

Different versions of Neretnieks' model can be found in the literature: the complete model (Moreno et al. 2010) and a simplified version developed by VTT (Finland), named the BESW model (Schatz et al. 2013). The BESW model consists in a simplification of the former for easing its implementation and convergence in COMSOL, with the diffusion coefficient and the sol viscosity being expressed as fitted correlations in terms of sodium cation and smectite concentrations. Moreover, the first model has been extended during the BELBaR project with a semiempirical two-region model for the computation of eroded mass at the rim. The development of this two-region model was motivated by the fact that the original continuous model failed to capture this phenomenon (Neretnieks et al. 2017).

Within the POSKBAR project, alternative approaches to Neretnieks' model were also explored. A novel method based on a particle-based approach using CFD-DEM (computational fluid dynamics and discrete element models) was developed by Laviña et al. (2018) but led to an excessive computational cost. Soil mechanics models based on the Barcelona Expansive Model were also applied, which failed to converge for very large strains due to the unsuitability of the constitutive model for reproducing large deformations and the boundary conditions considered. In this sense, a new soil mechanics model has been presented by Islam et al. (2019) for bentonite sealings of oil and gas wells. It also uses a swelling pressure correlation, but in this case, it is coupled with a plastic constitutive model for unsaturated soils. They furthermore modelled the bentonite-fracture contact shear strength for limiting the expansion into borehole fractures. A similar approach is presented by Börgesson et al. (2018), deriving an analytical expression for the penetration depth of bentonite

extrusion. In both cases, it shows a linear dependency with the fracture aperture. However, this behaviour is not observed in the laboratory tests presented by Alonso et al. (2019), which show similar expansion patterns for apertures ranging from 0.2 to 1 mm in cases considering stagnant low salinity waters.

In the present report, the scope of Neretnieks' model is extended to include other physical processes, such as fluid mechanics and surface tension, in an attempt to increase the level of understanding of some of the important phenomena behind bentonite expansion and erosion.

1.3 Limitations of Neretnieks' model

Neretnieks' model has succeeded in reproducing the physics behind bentonite expansion without resorting to casuistic approaches. However, in a strict sense, the model is only valid for free swelling, since it does not account for viscous forces due to confinement, for instance wall friction, that would limit the expansion of smectite paste in scenarios below CCC. In these cases, the model leads to an overestimation of the expansion (Neretnieks et al. 2017). This disagreement becomes even more significant with the BESW implementation of Neretnieks' model (Schatz et al. 2013) due to the overestimation of the diffusion coefficient at low smectite volume fractions (see Chapter 6). In this sense, the disagreements between the model results and experimental observations are not only related to the physical assumptions of the model, but also to the conceptual model behind bentonite expansion. This issue is related with the nature of the diffusion coefficient, which deals with the equilibrium between high force gradients at the nanoscale, yielding a significant concentration gradient at the expanding front. In cases without fracture flow, the bentonite transport is reduced to a diffusion equation, which under the presence of this force gradient will continue to expand indefinitely. Limiting the expansion of bentonite has previously been studied from different perspectives, including soil mechanics with wall friction (Börgesson et al. 2018), bentonite shear strength (Neretnieks and Moreno 2018b) and particle clogging (Richards 2010), but has not been assessed in Neretnieks' model yet.

From a chemical viewpoint, Neretnieks' model is limited to the effect of the sodium cation concentration on the expanding capacity of the clay. This is a simplification of all the chemical processes involved in the bentonite-fracture system, for which it can a priori only be applied to sodium homoionised bentonites in sodium chloride solutions. However, this approach can be considered as a worst-case estimator because commercial bentonites in contact with low salinity waters (i.e. glacial water) will absorb calcium, which is known for reducing the clay swelling capacity.

Another issue with Neretnieks' model is that erosion is significantly underestimated. There might be several reasons behind this disagreement which will be analysed in Chapter 4: the lack of shear stress in Darcy's law, the exclusion of the compacted bentonite pellet from the model domain, the 2D nature of the model, etc. In any case, Neretnieks' model provides a reduced interaction between sol and seeping water, which prevents erosion. A two-region model was developed to compensate this deficit and the results were significantly improved (Neretnieks et al. 2017). It consists in the solution of a second transport problem where the advective term coming from the flow equation is replaced by a sink computed from mass balance considerations, which in turn depends on an erosion rate that is estimated in a semi-empirical fashion using a previously obtained rim perimeter.

Finally, flocculation is the other key factor in the loss of bentonite that has not yet been included in the model, although significant efforts have been made at an experimental level for understanding the physical mechanisms behind this phenomenon (Neretnieks et al. 2017). The disaggregation of the sol during expansion is known to be driven by the chemistry of water and bentonite, but a sudden change in the fluid consistency due to non-linear effects could also explain flocculation from a mechanical point of view. In fact, gravity-driven cases show a higher flocculation ratio than horizontal test configurations (Neretnieks et al. 2017). This extension remains out of the scope of the present study but is briefly discussed in Chapter 8.

2 Objectives and scope

The final goal of the project is to develop a model that can be used to predict the expansion and erosion of saturated bentonite in a repository using transport and water flow equations in fractures. The mechanisms behind these phenomena have already been studied both experimentally and numerically (Neretnieks et al. 2017), observing considerable disagreements between the two approaches, mainly because of the unexpected importance of gravity, wall friction and flocculation in some cases.

At this first stage of the work, the scope of the study is limited to understanding the physical factors that limit expansion of saturated bentonite into fractures. Additionally, the erosion mechanisms due to seeping water flow are also preliminarily addressed. For this purpose, two versions of Neretnieks' model have been first implemented in COMSOL Multiphysics: Neretnieks' model proposed by Moreno et al. (2010) and the simplified BESW model (Schatz et al. 2013). The models have been tested to check the reported disagreements with experimental data regarding excessive expansion and underestimation of erosion (Neretnieks et al. 2017). Chapter 6 presents the results of the two implementations and the comparison with a test in Schatz et al. (2013) and the corresponding simulation performed by Neretnieks et al. (2017).

In Chapter 4, an extension of Neretnieks' model is presented, which is also implemented in COMSOL. The model results are compared with experimental data from simplified small-scale tests by Alonso et al. (2019). In spite of not resorting to full-scale realistic buffer conditions, this will allow a first evaluation of bentonite long-term integrity in buffer conditions for the safety assessment (SKB 2011). Given the relatively high level of uncertainty in the experimental measurements of eroded mass (Alonso et al. 2019), the performance in terms of bentonite erosion of the presented model is only analysed qualitatively at this stage.

The proposed extension of Neretnieks' model aims at adapting the original formulation, based on the hypothesis of free expansion, to a tightly confined medium. In very narrow fractures, wall friction, which is directly connected to swelling pressure, might play a key role in limiting the expansion of bentonite when low salinity waters intrude the deposition holes. Moreover, viscous effects such as shear strength of the dilute sol region could describe the physics behind erosion without resorting to empirical models. For this reason, the flow equations will be given special attention.

Another objective of this study is the quantitative estimation of the time at which concentrations below CCC in the vicinity of the buffer are reached after the exposure to glacial waters. This event could trigger high erosion rates which might compromise the integrity of the bentonite barrier (SKB 2011).

3 Methodology

The description of bentonite expansion and erosion consists in the coupling of three physical problems: sodium cation transport, smectite expansion and flow dynamics. All of them are solved in the computational platform COMSOL Multiphysics version 5.4 (COMSOL 2018) using the finite element method and a staggered scheme, which solves the three problems sequentially up to convergence in the above-mentioned order.

The sodium concentration in the bentonite porewater is not expected to change over the short time spans of the simulated tests (ranging from 19 to 30 days). In other words, the diffusion of sodium cation to the seeping water will not wash the bentonite out. On the other hand, the effects of other chemical species or accessory minerals on the chemical composition has not been considered either, although they might play an important role, especially in closed configurations such as the tests by Alonso et al. (2019). However, for long-term scenarios corresponding to realistic buffer configurations, the leaching of salts from the bentonite might trigger a massive erosion once the CCC is reached. For this reason, an extension of the sodium cation transport equation using two different solute transport models will be presented: a Fickian diffusion model based on the Multi-porosity model (Appelo 2013) and the Donnan equilibrium model (Birgersson and Karnland 2009), as applied for example in (Idiart and Coene 2019). Both approaches will be tested in Chapter 7 without any coupling with smectite expansion or flow equations.

The key feature of the smectite expansion equation in Neretnieks' model is the diffusion coefficient estimation, which relates expansion to the difference of repulsive and attractive force gradients at the nanoscale (Liu et al. 2009). This model was implemented in COMSOL to evaluate the limitations listed in Section 1.3 (it does not include the effect of external forces, such as wall friction). In Chapter 4, the model is extended with several features that aim to provide a more accurate description of bentonite expansion in rock fractures and erosion mechanisms due to low salinity groundwater intrusion.

Regarding the conceptual model of flow dynamics, it is proposed here to include wall friction, swelling pressure and a non-Newtonian rheology to provide a physically consistent approach to the simulation of bentonite erosion. This is presented in Chapter 4. Although the performance of this model has not yet been analysed, three simplified alternatives based on the Brinkman and Stokes equations are tested in a case with a high seeping water flowrate (Chapter 6).

A total of fourteen simulations, listed in Table 3-1, have been computed with the proposed model for validating its performance in terms of bentonite expansion and erosion against experimental data from Schatz et al. (2013) and Alonso et al. (2019). The results are presented in Chapter 6.

In turn, the two models describing the porewater salinity evolution in the vicinity of the buffer when glacial water intrudes the repository are presented in Section 4.5.1 and the corresponding results are analysed in Chapter 7, with twelve additional simulations (Table 3-2).

Table 3-1. List of bentonite expansion and erosion simulation cases analysed in Chapter 6. Reference [1]: Alonso et al. (2019); reference [2]: Schatz et al. (2013). Version 1 and 2 correspond to models without and with wall friction and surface tension effects, respectively. K-C and M-K-C correspond to Kozeny-Carman and Modified Kozeny-Carman relations between porosity and permeability, respectively.

Test	Reference	Model	Version	Fracture width (mm)	Dissolved Na (mM)	Flow (m/s)
4B	[1]	Proposed model	1	0.1	1	0
			2	0.1	1	0
6B	[1]	Proposed model	1	0.2	1	0
			2	0.2	1	0
8A	[1]	Proposed model	1	0.4	1	0
			2	0.4	1	0
52A	[1]	Proposed model	1	1	1	0
			2	1	1	0
11	[2]	Neretnieks' model	-	1	0.03	0
11		BESW	-	1	0.03	0
3	[2]	Neretnieks' model with K-C Brinkman flow	1	1	0.03	2×10^{-4}
		Neretnieks' model with M-K-C Brinkman flow	1	1	0.03	2×10^{-4}
		Viscosity-scaled Brinkman flow	1	1	0.03	2×10^{-4}
		Stokes flow	1	1	0.03	2×10^{-4}

Table 3-2. List of salt leaching simulation cases analysed in Chapter 7.

Case #	Model	Flow (m/yr)
A1	Fickian diffusion in free porosity	10^{-5}
A2	Fickian diffusion in free porosity	10^{-4}
A3	Fickian diffusion in free porosity	10^{-3}
A4	Fickian diffusion in free porosity	10^{-2}
A5	Fickian diffusion in free porosity	1.1×10^{-1}
B1	Fickian diffusion with reduced free porosity	10^{-5}
B2	Fickian diffusion with reduced free porosity	10^{-4}
B3	Fickian diffusion with reduced free porosity	10^{-3}
B4	Fickian diffusion with reduced free porosity	10^{-2}
B5	Fickian diffusion with reduced free porosity	1.1×10^{-1}
C1	Donnan model	1.0×10^{-5}
C2	Donnan model	1.1×10^{-1}

4 Description of conceptual model

4.1 Model geometry

The experimental setups developed by Alonso et al. (2019) and Schatz et al. (2013) are shown schematically in Figure 4-1. In both cases, the assembly includes a planar fracture between two plates, which contain an encapsulated pellet of compacted bentonite.

The only differences between the two setups are the dimensions of the plates (17cm × 17 cm and 24 cm × 24 cm in Alonso et al. (2019) and in Schatz et al. (2013), respectively), the diameter of the bentonite pellet (1.9 vs 2.0 cm), its height (1.0 vs 2.0 cm) and its initial dry density (1 400 vs 1 591 $kg \cdot m^{-3}$).

A full three-dimensional representation of the experiments is considered in this work, without assuming any symmetry plane, in order to account for configurations with flow, slope and roughness in future stages of the study.

4.2 General principles

This modelling study stems from the model for bentonite expansion and erosion proposed by Liu et al. (2009), Moreno et al. (2010) and Neretnieks et al. (2009). In the present work, some modifications and extensions of the model are proposed following two general principles: (1) continuity, including the solution in compacted bentonite, and (2) stronger coupling between the field equations for physical consistency. The first one refers to the necessity of simulating the real motion of the expanding paste and sol, as well as the shear velocity at the rim region for a better assessment of the balance between expansion and erosion. In this sense, the Darcy equations used by Neretnieks et al. (2017) significantly underestimate erosion, even for high flowrates, unless relying on aprioristic rim concentration values. For this reason, alternative flow models based on the Stokes and Brinkman equations are proposed. The second principle aims at reproducing the fundamental physics behind bentonite expansion and erosion, limiting the use of casuistic approaches and striving forward to a physical unification. This implies that the water flow and smectite expansion equations need to be more intimately coupled. For example, swelling pressure will be included in the flow equations and wall friction is assumed to affect the smectite transport.

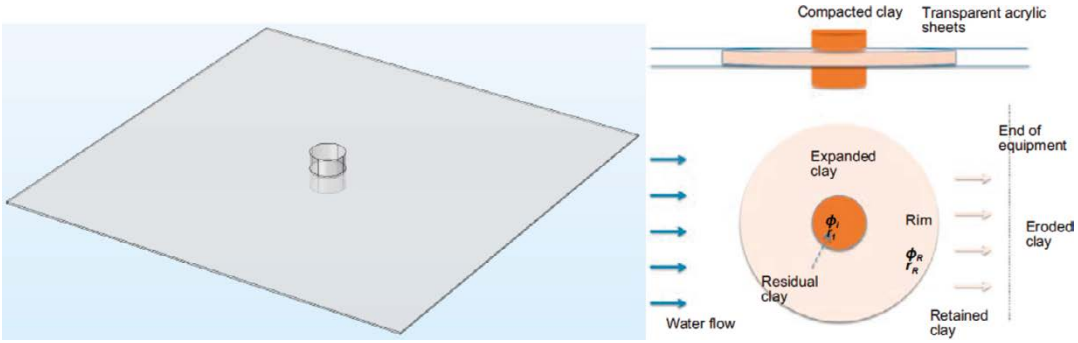

Figure 4-1. *Schematic conceptual model with a planar fracture cutting through a cylindrical bentonite pellet (Neretnieks et al. 2017).*

4.3 Flow dynamics

4.3.1 Brinkman and Stokes equations

Equation 4-1 shows the general form for fluid flow in porous media. The Neretnieks flow model is limited to Darcy's law, which is given by the last two terms of this equation and constitute the most widely used approach to laminar flow in porous media. With that approach, the fluid and the solid matrix remain as clearly separate phases. However, the studied system does not fulfil this hypothesis because the seeping water progressively changes the rheological properties of the expanding bentonite front. This leads to two specificities: on one hand, the appearance of viscous effects related to wall friction due to the expanding paste, and on the other, the interaction of seeping water with the dilute sol, which can trigger an erosion process. For these two reasons, shear stress effects need to be considered and therefore the diffusive viscous term (second term in Equation 4-1) is added to Darcy's law, obtaining the so-called weakly compressible Brinkman equations (Badia and Codina 2009). Although seeping water flow is considered incompressible and conservation of mass is assumed, the continuity equation (Equation 4-3) allows water storage in the expanding clay in a similar way as for two-phase flow:

$$\rho\partial_t\vec{u} - \nabla\cdot\tau + \nabla p - \eta\kappa^{-1}\vec{u} = \vec{0} \qquad \text{Equation 4-1}$$

$$\tau = \eta_{eff}\nabla^S\vec{u} \qquad \text{Equation 4-2}$$

$$\partial_t(\rho\varepsilon) + \nabla\cdot(\rho\vec{u}) = 0 \qquad \text{Equation 4-3}$$

In these equations, ε is the porosity (-), ρ is the fluid density (kg·m^{-3}), η is the dynamic viscosity (Pa·s), κ is the medium permeability (m^2), $\vec{u}$ is the velocity (m·s^{-1}) and ρ is the pressure (Pa). Equation 4-2 states the relation between shear stress, τ, and the effective viscosity, η_{eff}, presented in Section 4.3.3, and the strain rate $\nabla^S\vec{u}$ (∇^S being the symmetric gradient), also referred to as $\dot{\gamma}$, which corresponds to the symmetric velocity gradient tensor. Neretnieks' model uses the Kozeny-Carman correlation for the term f (kg · s^{-1}) described in Section 4.4, which accounts for the friction between seeping water and the solid fraction. This term penalizes the diffusivity function χ (J) in the smectite transport equation (Equation 4-11 in Section 4.4). In order to be consistent with this modelling approach, the permeability-porosity constitutive relation of bentonite in the Darcian term of the flow equation (fourth term in Equation 4-1) has been tentatively defined accordingly:

$$\kappa = \frac{(1-\varphi)^3 a_s}{k_0\varphi^2} \qquad \text{Equation 4-4}$$

where φ is the smectite volume fraction (-) for which $\varepsilon = 1-\varphi$, a_s is the surface area of the smectite sheet and k_0 is the Kozeny constant. However, this relation does not necessarily apply to dilute sols and is independent of the fracture permeability ($\delta^2/12$), δ being the fracture aperture. Figure 4-2 shows how the permeability does not reach that of the fracture (8.33×10^{-8} m^2 assuming a 1 mm aperture) when the smectite volume fraction tends to zero. On the other hand, the Kozeny-Carman relation could overestimate the permeability at low bentonite concentrations if the fracture aperture is reduced to e.g. 0.1 mm ($\delta^2/12 = 8.33\times10^{-10}$ m^2).

A possible solution to this disagreement could consist in using a modified Kozeny-Carman relation that explicitly considers the fracture properties. Höglund (2014) proposed a log-log relation that forces a specified permeability value when the dependent variable (in this case the smectite volume fraction) tends to zero. In this way, the permeability curve can be forced to reach the fracture permeability when φ tends to zero, although the difference does not seem significant a priori for 1 mm apertures (see Figure 4-2).

A third approach for the permeability correlation of the flow equations is found in Moreno et al. (2010), which has been used for the cases simulated in Neretnieks et al. (2017) instead of resorting to a Kozeny-Carman model. In this case, the permeability of smectite is derived from a given transmissivity of the fracture by scaling with the relative viscosity as $\kappa = \kappa_0/\eta_{rel}$. In their simulations, $\kappa_0 = 10^{-11}$ m^2 for the open fracture, according to Sawada et al. (2001), and η_{rel} follows a cubic correlation with φ, as proposed by Adachi et al. (1998). More details can be found in Appendix A. This alternative provides a similar value for the most dilute sol but keeps permeability quite constant up to a value of $\varphi = 0.01$ (Figure 4-2), making it more permeable to seeping water and thus increasing the erosion potential. However, as will be shown in Chapter 6, Neretnieks' model using the Darcy equation with this alternative correlation for permeability fails in capturing erosion, even in cases

with high water flowrates (Neretnieks et al. 2017). For this reason, a solution to this issue was presented in the same work, where a rim concentration φ_R (-) is assumed *a priori* as a fixed value where erosion takes place. A second smectite transport problem needs to be solved in this outer region, replacing the convective term coming from the flow equations for a sink term coupled with a mass balance equation. The erosion rate $N_{erosion}$ (kg·s^{-1}) is modelled with the following expression:

$$N_{erosion} = \rho_s \delta \varphi_R \frac{4}{\sqrt{\pi}} \sqrt{D_R \pi r_R u_0}, \qquad \text{Equation 4-5}$$

where D_R is the diffusion coefficient at the rim (m^2·s^{-1}), r_R the expansion radius (m), μ_0 is the approaching water velocity (m·s^{-1}), ρ_s is the smectite particle density (kg·m^{-3}) and δ is the fracture aperture (m). This method requires tracking the rim region at $r_R(t)$ and defining an appropriate φ_R for each scenario. In some cases, it overestimates erosion (Neretnieks et al. 2017), and in others, such as gravity driven tests, it fails in capturing erosion above rim concentration.

Based on the above, it seems justified to strive towards a model of bentonite erosion that only relies on physical principles. At this stage, the presence of the rheological model only affects the outermost dilute sol (with a high permeability), which may interact with seeping water and move accordingly. Due to the sharp viscosity increase with smectite volume fraction, the corresponding low permeability will immobilize the gel and the paste. An alternative consists in the simpler Stokes problem, that gets rid of the permeability term. Indeed, the Stokes equation results from Equation 4-1 if the contribution of the fourth term is neglected. This approach, combined with an appropriate rheological model, could have the interesting side effect of describing the dynamics of paste, sol and water in a continuous fashion as a slurry flow, relying only on shear resistance for balancing inertial forces. As will be shown in Chapter 6, this leads to an overestimation of the interaction at the rim region and thus an excessive erosion rate, which in turn does not allow bentonite to expand. However, this approach may be regarded as a worst-case scenario and will show the relevance of the balance between expansion and erosion in cases with considerable flow rates.

Finally, the permeability model in Moreno et al. (2010) has been used in combination with the Brinkman equations in order to evaluate the importance of solving both transport and flow equations in the whole domain, i.e. including the compacted bentonite region. Unlike the Darcy's law used in Neretnieks' model, in this case viscous shear stresses are accounted for. Although this provides a more accurate equilibrium between expansion and erosion than the single Stokes equations, it still underestimates the former in favour of the latter. However, as discussed in Chapter 6, the important outcome of this last model is the suitability of the Brinkman equations for simulating erosion due to the relevance of the viscous shear term.

For all these reasons, the effect of considering the swelling pressure in the Stokes/Brinkman equation on the resistance to erosion is explored next.

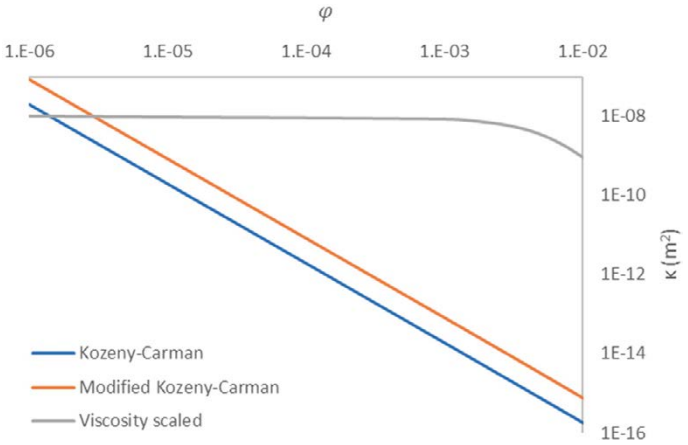

Figure 4-2. *Permeability κ (m^2) vs. smectite volumetric fraction φ (m^3·m^{-3}) as calculated with the Kozeny-Carman model, the log-log modified correlation by Höglund (2014) and a viscosity-scaled curve used in Moreno et al. (2010) for a fracture aperture of 1 mm.*

4.3.2 Swelling pressure

So far, the impact of swelling pressure and the resulting motion of the smectite paste on the flow equation has not been explicitly considered. In Neretnieks' model, swelling pressure is calculated as the difference between the gradient of interparticle diffuse double layer (DDL) repulsive force and the attractive van der Waals force (e.g. Karnland et al. 2005). However, bentonite deformation velocity and the subsequent paste and sol motion are not explicitly considered in the flow equations. Instead, the effects of bentonite deformation on flow are only considered indirectly through the effect of a change in viscosity of the fluid due to bentonite mass increase on fracture transmissivity (Moreno et al. 2010).

The coupling between flow equations and swelling model assumes that the pressure gradient in the original formulation only refers to the seeping water but does not describe the high pressure gradients within the swelling paste. This aspect is crucial in order to derive the real stress – strain state of the slurry flow, which will allow obtaining the shear resistance needed for limiting diffusion in the transport equation (Section 4.4.1). For this reason, the clay swelling pressure gradient is explicitly considered in the flow momentum equation (see Equation 4-6). The large viscosities in the paste will avoid mobilization, but near the rim, this radial force pointing outwards might play an important role in the simulation of the pseudo-equilibrium between erosion and expansion observed in test 3 (Schatz et al. 2013).

Bentonite motion plays a key role in cases where expansion and erosion occur simultaneously and where these two processes may reach equilibrium, such as test 3 in Schatz et al. (2013). This test is simulated in the present work using Neretnieks' model, and the results are presented in Chapter 6. Rigorously, it would be necessary to consider swelling pressure effects for providing the proper shear stresses and strains of the water-bentonite mixture, as well as the expansive inertial force. This could be crucial for obtaining a realistic resistance to erosion at the interface with seeping water. As a hydrostatic force, swelling pressure, p_{sw}, can simply be added to the flow pressure in Stokes equation, for which its gradient becomes a force term (Equation 4-6):

$$\rho \partial_t \vec{u} - \nabla \cdot \tau + \nabla(p + p_{sw}) = \vec{0} \qquad \text{Equation 4-6}$$

At the expansion front, before reaching the equilibrium between DDL and van der Waals forces, the high smectite concentration gradient leads to a strong swelling pressure gradient (∇p_{sw}), which should be compensated towards the mechanical equilibrium by an expansion velocity of the paste ($\vec{v}_{\text{exp}}$). This velocity vector, pointing radially outwards (Figure 4-3), will in turn affect the balance between expansion and erosion in cases with significant fracture water flow (see Chapter 6).

The development of an alternative flow formulation including features such as swelling pressure, non-Newtonian and viscous effects has not been yet completed. In fact, the rheological model is still to be implemented. However, this model is conceived to be the basis for the coupled simulation of cases with water flow involving erosion, since it will provide an enhanced representation of the interaction between seeping water and dilute sol.

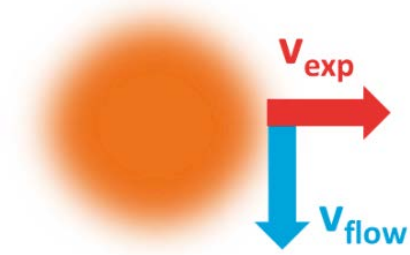

Figure 4-3. *Schematic representation of the balance between bentonite expansion and erosion.*

4.3.3 Dry and viscous wall friction forces

In the previous subsection, the flow model has focused on describing scenarios with fracture water flow where expansion and erosion would tend to balance each other until reaching a pseudo-steady state. However, when considering the case of bentonite expansion in contact with stagnant low salinity groundwater (below CCC), mechanical erosion is not an issue anymore. The main question regarding the long-term stability of the bentonite buffer, is thus whether the smectite gel will expand indefinitely or whether it could stop by some sort of resistance to motion. Experimental results show both possibilities: on one hand, Alonso et al. (2019) found a bounded expansion with $[Na^+]$ = 1 mM, whereas Schatz et al. (2013) did not observe steady state conditions when using deionized water. However, it should be noted that the salinity of the solution in the fracture increased above the CCC during the experiments of Alonso et al. (2019). At this stage of the study, the potential role of sedimentation and clogging of relatively large accessory mineral particles will not be analysed. Instead, focus is made on the role of wall friction.

One of the main challenges is to capture with a single model the behaviour of the solid and fluid phases simultaneously. Whereas the behaviour of compacted bentonite has been traditionally studied from the soil mechanics perspective (e.g. Gens 2010), dilute gel and sol have been modelled as non-Newtonian fluids (Neretnieks and Moreno 2018b). If the problem is restricted to a solid extrusion (e.g. Börgesson et al. 2018) and a balance is derived between swelling pressure and the static friction stress ($2\mu p_{sw}$), the expansion distance can be shown to be directly proportional to the fracture aperture, δ (m). This result disagrees with the experimental tests performed by Alonso et al. (2019), which show that the final expansion does not increase significantly in the range δ = 0.2-1.0 mm. One way to remedy this is to consider the viscous shear stresses (τ, in Pa) of the fluid phase in Equation 4-1 as well as its nonlinear effects:

$$\rho\partial_t\vec{u} - \nabla\cdot\tau + \nabla\big(p + p_{sw}(1-2\mu)\big) = \vec{0}, \qquad \text{Equation 4-7}$$

where μ (-) is the friction coefficient between the expanding bentonite and the fracture wall derived by Åkesson et al. (2010), and τ can be expressed according to a Herschel-Bulkley model for non-Newtonian fluids, which has been fitted by Pujala (2014):

$$\tau = \tau_0 + k_{HB}|\dot{\gamma}|^n, \qquad \text{Equation 4-8a}$$

$$\tau_0 = 0.2\left(100\frac{\varphi\rho_s}{\rho}\right)^3 \qquad \text{Equation 4-8b}$$

where τ_0 (Pa) is the yield (or mobilization) shear stress, which is the minimum stress needed for mobilizing the smectite paste, $\dot{\gamma}$ is the strain rate (s^{-1}) and k_{HB} ($Pa\cdot s^n$) and n (-) are the two parameters of the model, which are defined as n = 0.45 and

$$k_{HB} = 130\frac{\varphi\rho_s}{\rho} - 2.3, \qquad \text{Equation 4-9}$$

where φ is the smectite volume fraction (-), ρ_s is the solid or grain density ($kg\cdot m^{-3}$), and ρ is the bulk density ($kg\cdot m^{-3}$).

Non-linear effects have already been observed in very dilute suspensions (Pujala 2014), for which this regression of the Herschel-Bulkley model is proposed for the whole domain:

$$\eta_{eff} = \eta_0 = \tau_0|\dot{\gamma}_0|^{-1} \text{ if } |\dot{\gamma}| \le \dot{\gamma}_0 \qquad \text{Equation 4-10a}$$

$$\eta_{eff} = \tau_0|\dot{\gamma}|^{-1} + k_{HB}|\dot{\gamma}|^{n-1} \text{ if } |\dot{\gamma}| > \dot{\gamma}_0 \qquad \text{Equation 4-10b}$$

This formulation is thought to be suitable to represent the phenomenology behind the motion and erosion of smectite gel and sol. Additionally, it allows to estimate the strain rate ($\dot{\gamma}$) during expansion, which could be used in the future for the implementation of a flocculation model based on Sato et al. (2004). As observed in Neretnieks et al. (2017), flocculation takes place already during expansion and is closely related to water chemistry (sol consistency) and fracture aperture. Thus, the non-linear strain rate might play an important role in this phenomenon.

4.4 Smectite transport

The transport of smectite due to swelling in low salinity water is described by Liu et al. (2009), which derives the diffusion coefficient as the quotient of a diffusivity function, χ (J), and a friction factor, f (kg·s^{-1}). The former expresses a force balance at the nanoscale between DDL repulsive and van der Waals attractive forces. The friction factor acts as a penalty function due to frictional forces between water and smectite sheets (see Appendix A). This model is of key importance for providing a physically based smectite expansion equation in terms of volume fraction (φ). It is also essential to calculate the key parameters of the flow equations – density, viscosity and swelling pressure – and ensuring a proper coupling between both physics.

$$\partial_t \varphi + \vec{u} \cdot \nabla \varphi - \nabla \cdot \left(\frac{\chi}{f} \nabla \varphi \right) = 0 \qquad \text{Equation 4-11}$$

In the present study, the previous coupling is preserved, but in line with the presented general principles, the smectite expansion equation covers the whole domain in a continuous fashion. It is noted that the smectite volume fraction at the interior of the bentonite pellet could decrease with time, even for short test durations. Moreover, in consonance with the implemented wall friction model for the flow equations (Section 4.3), in the next section (see Equation 4-16) a convective term is included in the smectite transport equation to establish a force balance between diffusion (which drives the expansion) and the joint effect of static friction and viscous shear (which restrict the expansion). In cases with water flow, this equilibrium might be provided by erosion, but in stagnant cases Neretnieks' model does not provide a counteracting force that limits free swelling, which will continue for as long as the diffusivity function is larger than zero and there is a non-zero smectite concentration gradient (Neretnieks et al. 2017).

4.4.1 Wall friction force and shear resistance

One of the main features in the process of physical unification of both flow and smectite transport equations is the consideration of wall friction effects. According to Kanno et al. (2001), these effects are clearly visible when bentonite swells in fractures with an aperture of less than 1 mm. The quantification of this resistance against diffusion is a key aspect for a more realistic estimation of the total extruded bentonite mass after 100k or 1M years. At this point, it must be noted that the extension of Neretnieks' model will not focus on the diffusion coefficient proposed by Liu et al. (2009), which has proved to describe the physics of smectite expansion quite accurately (see Section 6.1). Instead, an additional term is proposed in the smectite transport equation to compensate expansion in cases where wall friction effects are expected, and erosion does not take place (no external flow).

According to Liu et al. (2009), the force balance behind smectite transport can be written as follows:

$$\vec{F}_\eta = -\vec{F}_s - \frac{\chi}{\varphi} \frac{\partial \varphi}{\partial \vec{x}}, \qquad \text{Equation 4-12}$$

where $\vec{F}_\eta$ refers to the frictional force between phases, $\vec{F}_s$ to the gravity and buoyancy forces and φ to the smectite volume fraction. The frictional force $\vec{F}_\eta$ can be expressed in terms of the expansion velocity as $\vec{F}_\eta = f\vec{v}$. In this way a smectite flux can be defined as $\vec{J} = \varphi\vec{v}$, which after some algebra leads to the following equation (Liu et al. 2009):

$$\vec{J} = -\frac{\vec{F}_s \varphi}{f} - \frac{\chi}{f} \frac{\partial \varphi}{\partial \vec{x}} \qquad \text{Equation 4-13}$$

Mass conservation then reads:

$$\partial_t \varphi = -\nabla \cdot \vec{J} \qquad \text{Equation 4-14}$$

At this point, we redefine the frictional force $\vec{F}_\eta$ by adding a wall friction velocity ($-\vec{w}$) to the expansion velocity $\vec{v}$, reading:

$$\vec{J} = \vec{w}\varphi - \frac{\vec{F}_s \varphi}{f} - \frac{\chi}{f} \frac{\partial \varphi}{\partial \vec{x}} \qquad \text{Equation 4-15}$$

After imposing mass conservation and neglecting for the moment the gravity and buoyancy forces $\vec{F}_s$, the smectite transport equation with wall friction is obtained:

$$\partial_t \varphi = -\nabla \cdot (\vec{w}\varphi) + \nabla \cdot \left(\frac{\chi}{f} \nabla \varphi \right) \qquad \text{Equation 4-16}$$

The friction force is implicitly included in the wall friction velocity and appears as a conservative advective term in Equation 4-16 that can be directly implemented in the numerical model. However, $\vec{w}$ still needs to be defined. In fact, it is a virtual velocity that quantifies the resistance to expansion at each point of the domain. In order to be consistent with the presented fluid mechanics equations for a laminar viscous flow (see Equations 4-7 and 4-8), $\vec{w}$ can be defined as the average velocity of a viscous laminar flow between two parallel plates, as if wall friction and shear stress were the driving traction:

$$\vec{w} = \frac{(2\mu p_{sw} + \tau_0)\delta}{4\eta_{eff}} \qquad \text{Equation 4-17}$$

where δ (m) is the fracture aperture and η_{eff} is the effective viscosity given in Equation 4-10. In cases without flow, the Stokes equations are not solved, so that the strain rate needed to calculate the effective viscosity is unknown. Thus, the shear stress is simplified to τ_0, i.e. the yield shear stress of the material. This assumption is consistent with the case under study, since flocculation and gravity, which might involve high strain rates, are not considered at this point. Physically, this term represents the resistance of gel against shear deformation, which would also appear in a hypothetical scenario of unconfined swelling. Therefore, the effective viscosity becomes $\eta_{eff} = \tau_0 \dot{\gamma}_0^{-1}$ and plays an important role in the scaling of $\vec{w}$. The effect of sand-like accessory particles on the expansion of the clay, analysed in Neretnieks and Moreno (2018a, b), which could involve solid friction with the fracture walls, has not yet been included in the model. Up to now, only the behaviour of homoionised montmorillonite has been analysed.

It should be noted that the term δ in Equation 4-17 penalizes the expansion for wider apertures, which a priori is not physically sound. However, it is reasonable to assume that η_{eff} will also increase proportionally with δ because in laminar viscous flows the velocity profile shows a parabolic shape, while shear stress and strain have a linear profile (Equation 4-2). This means that, considering an average expansion velocity v_{exp}, the mean mobilization strain rate will be $\dot{\gamma}_0 \sim \frac{v_{exp}}{\delta}$. In that case, δ cancels out in Equation 4-17. Therefore, in this first approach $\vec{w}$ will not depend explicitly on δ. However, two ingredients might provide a more accurate representation of η_{eff}: on one hand the coupled calculation of Equation 4-7, which would yield a realistic strain rate distribution, and on the other, the availability of a valid rheological model for the whole operational range, at least regarding τ_0. In this sense, the correlation for a Herschel-Bulkley model provided by Pujala (2014) in Equations 4-8 and 4-10 corresponds to measurements for dilute bentonite suspensions, but no assessment regarding denser conditions has been found in the literature. For this reason, the wall friction term in Equation 4-17 has been restricted to $\varphi < 0.1$. In Chapter 6 it will be analysed whether this simplification is consistent with the behaviour of friction and diffusion observed by Alonso et al. (2019).

Another important parameter of the present model is the friction coefficient μ. Although the correlation proposed by Åkesson et al. (2010) with α/2, being α the friction angle, as shown in Börgesson et al. (2018), which yields the best fitting with the triaxial tests performed by Börgesson et al. (1995), has been adopted, it has been limited to $\varphi > 7.0 \times 10^{-3}$. Around this concentration, swelling pressure and yield shear stress are already negligible, and so is wall friction, whereas diffusivity is still significant due to the presence of the expansion front (high concentration gradient). This means that a relevant portion of dilute sol could expand indefinitely. Nevertheless, a relevant force appears at the interface between this dilute sol and seeping water due to the surface tension differential, which according to Schramm and Hepler (1994) has been measured in 2 mN·m^{-1}. In this sense, Girifalco and Good (1957) provided the following analytical expression of the interfacial tension σ_{int} (N·m^{-1}) between two phases *a* and *b*:

$$\sigma_{int} = \sigma_a + \sigma_b - 2\Phi\sqrt{\sigma_a \sigma_b} \qquad \text{Equation 4-18}$$

This tension is very sensible to the parameter Φ, which has been estimated for liquid-solid interfaces but is not so properly defined for liquid-liquid interactions (Jańczuk et al. 1996), for which the surface tension differential has been directly taken as the interfacial tension (σ_{int} =2 mN·m^{-1}) as first guess. Then, the resulting stress on the outer surface of the sol τ_σ (Pa) will be

$$\tau_\sigma = \frac{2\sigma_{int}}{\delta} \qquad \text{Equation 4-19}$$

Bearing in mind the small fracture apertures δ under consideration ($< 1 \times 10^{-3}$ m), this force might be large enough to play an important role in the force balance at the expansion front. In fact, it is considered one of the driving forces in microfluidics, where pressure ranges and gravitational forces tend to be negligible with decreasing δ (Vowell 2009). Then, Equation 4-17 becomes

$$\vec{w} = \frac{(2\mu p_{sw} + \tau_0)\delta}{4\eta_{eff}} \text{ if } \varphi > 7.0 \times 10^{-3} \quad \text{Equation 4-20a}$$

$$\vec{w} = \frac{2\sigma_{int}}{4\eta_{eff}} \text{ if } \varphi \leq 7.0 \times 10^{-3} \quad \text{Equation 4-20b}$$

This development will contribute, in a first stage, to the simulation of purely expansive scenarios (stagnant water). After further investigation on the wall friction mechanisms between smectite and fracture walls, which may also be tightly related to the rheological model, this contribution will be coupled with the flow equations in order to simulate cases with low flow rates and flocculation. Otherwise, an overestimation of the expansion might lead to wrong results in terms of long-term smectite losses.

4.5 Sodium transport

The sodium cation transport from bentonite to seeping water is based on a simple Fickian diffusion law which only considers salinity due to the presence of NaCl (no exchange with other cations is included) but omits the contribution of [Cl^-] based on electroneutrality. Moreover, the evolution of the bentonite chemistry does not affect the diffusion coefficient. Advective transport is also included in the model.

$$\partial_t c = \nabla \cdot (D \nabla c) - \vec{u} \nabla c \quad \text{Equation 4-21}$$

$$D = D_0 (1 - \varphi)^{1.6} \quad \text{Equation 4-22}$$

where c (mol·m^{-3}) is the solute concentration, $\vec{\mu}$ (m·s^{-1}) corresponds to the flow velocity vector, φ refers to the smectite volume fraction, D_0 (m^2·s^{-1}) is the diffusion coefficient of [Na^+] in water and D (m^2·s^{-1}) is the effective diffusion coefficient in bentonite. These simplifications are thought not to represent a significant limitation for the cases tested in Chapter 6 due to their relatively short temporal scope. The most relevant parameter is the initial sodium concentration in saturated bentonite, which can be obtained from literature (e.g. Bradbury and Baeyens 2003) and from the final water composition in experimental tests (Alonso et al. 2019). For all these reasons, Equations 4-19 and 4-20 are not solved in the compacted bentonite region and a Dirichlet boundary condition is prescribed on the pellet external boundary instead.

Although sodium transport is not solved for in the inner bentonite pellet domain, high smectite concentrations are expected to appear within the fracture near the boundary. For this reason, it makes sense to adapt Equation 4-21 to this scenario, which is not properly described by the present exponent for Archie's law. The implemented alternative corresponds to the model developed by Appelo (2013), which also includes a retardation factor due to cation exchange reactions, when applicable (Equation 4-23):

$$D = \frac{(1-\varphi)^{1.5} D_0}{(1-\varphi) + 10^{-2} \rho_d} \quad \text{Equation 4-23}$$

where ρ_d (kg·m^{-3}) is the bentonite dry density.

4.5.1 Solute transport in compacted bentonite

The transport of cations and anions from compacted bentonite to the fracture seeping water is an important issue when dealing with the long-term safety assessment (SKB 2011). The intrusion of glacial water in the selected sites of Forsmark (Sweden) and Olkiluoto (Finland) is one of the major concerns regarding the integrity of the bentonite buffer. Such scenario might trigger the erosion of the bentonite barrier once the concentration at the buffer – fracture interface drops below CCC. Soon after the glacial water reaches the buffer, leaching of soluble salts in the short term from the buffer towards the fracture will affect the salinity of the water in the vicinity of the buffer. However, it has not been clearly assessed yet how long it will take for equilibrium to be reached between the bentonite and glacial water and to dissipate the corresponding plume, which would temporarily prevent clay disaggregation.

On the other hand, the CCC criterion for MX-80 bentonite is not as clear as for homoionic Na-clays in NaCl dilutions, where the threshold can be more readily defined as the equilibrium between DDL repulsive and van der Waals attractive forces between particles (Liu et al. 2009). In the present case, where accessory minerals and the progressive cation exchange will lead to a Ca-rich bentonite, the significant presence of divalent ions will tend to stabilize the system. In this sense, Birgersson et al. (2009) experimentally determined the CCC to be 1–4 mM charge equivalents for mixed Na/Ca smectite containing 20–75% calcium. This criterion has been adopted for the KBS-3 repository safety assessment (SKB 2011).

Smectite is known for conserving the cationic charge in the interlayer (ion exchanger) which compensates its structural negative charge. In this regard, Cronstrand (2016) studied the integrity of the bentonite buffer under the effect of highly alkaline waters from concrete degradation, including cation exchange processes, showing a high percentage of sodium retention after 30k years. Similar results have been provided by Bruno and Duro (1999) with a near-field hydrochemical model for bentonite – water interaction using Aspö and Finnsjön groundwater compositions. In these cases, sodium bentonite was converted into calcium bentonite after 0.5 and more than 2 million years, respectively. However, experimental measurements in Muurinen and Lehikoinen (1999) and Alonso et al. (2019) reveal that significant salt leaching can take place at early stages of water intrusion. From a modelling perspective, these two processes have been assessed using different approaches. On one hand, considering single intergranular (free) porosity transport as presented in the previous section. On the other hand, using the Donnan approach (Birgersson and Karnland 2009) which restricts ionic transport in compacted bentonite to the interlayer porosity with an electroneutrality constraint. In the present work, the diffusion coefficient of the first approach is adapted to the presence of interlayer and DDL volume fractions, which leads to a reduction of the free porosity as proposed in the Multi-porosity model (Appelo 2013).

The main differences between the approaches are the porosity (or porewater) types considered and, as a result, the effective diffusion coefficients and available porosities estimated. The total porosity ϕ_{tot} of compacted bentonite can be calculated from the expression $\phi_{tot} = 1 - \rho_d \cdot \rho_s^{-1}$, where ρ_d is the dry density (kg·m^{-3}), i.e. the mass of clay (without hydration water) per unit total volume, and ρ_s (kg·m^{-3}) is the smectite grain density. Several authors have proposed to divide this total porosity into two or even three porosity (or porewater) types to model ionic transport in compacted bentonite (e.g. Bourg et al. 2003, Wersin 2003, Wersin et al. 2004, Muurinen et al. 2007). Bradbury and Baeyens (2003), for instance, suggested three different types of water in bentonite pores: free pore water, interlayer water and electrical double layer (EDL) water. The free pore water is a charge balanced aqueous solution of cations and anions. Interlayer water is found between smectite layers and contains water and cations, compensating the structural charge deficit of smectite layers. EDL water, on the other hand, present between the mineral surface and the free water, contains water, cations and a small number of anions. The excess of cations balances the remaining charge at the outer surface of the smectite. The relative portion of each porewater type depends on the degree of bentonite compaction (dry density), the salinity of the solution, and the amount of accessory minerals.

The two considered models have been chosen in order to bound the estimated leaching: an optimistic one corresponding to the Donnan model, which limits the solute transport to cation exchange processes, and a more pessimistic Fickian diffusion through free porosity, which does not account for the compensation of structural negative charge. The complete Multi-porosity model has not been implemented due to its high complexity for a multi-component system. In a previous implementation presented in Idiart and Coene (2019), transport was limited to a single radionuclide ($^{36}Cl^-$) through the bentonite backfill and was simulated with a constant background solution. The present scenario would involve the coupled transport of several species in a medium with time-evolving porosity (due to ionic strength changes) and solute distribution ratios. Therefore, the partition of the mass of ions between different porosity types could not be assumed as constant. This would lead to a highly complex model implementation, which in turn must cover a long temporal span, thus probably requiring long computation times.

This simplified Fickian approach, presented in Equations 4-24 and 4-25, will account for the initial leaching of ions stored in the free porewater, but does not provide any retention mechanism in terms of mineral or cation exchange reactions. The relation between cation leaching and free porosity, which depends on the porewater ionic strength, will be analysed in Section 7.1.

$$\varphi_{free}\partial_t c_i = \nabla \cdot (D\nabla c_i) - \vec{u}\nabla c_i \text{ in } \Omega. \qquad \text{Equation 4-24}$$

$$D = D_w \tau \varphi_{free}, \quad \text{Equation 4-25a}$$

$$\varphi_{free} = \varphi_{tot} - (\varphi_{DDL} + \varphi_{IL}), \quad \text{Equation 4-25b}$$

where c_i is the concentration of the i-th ion (mol·m^{-3}), φ_{tot}, φ_{free}, φ_{DDL} and φ_{IL} are the total, free, DDL and interlayer porosities (-), respectively, $\Omega = \Omega_b \cup \Omega_f$ is the total domain composed by the bentonite buffer (Ω_b) and the fracture (Ω_f), D is the effective diffusion coefficient of all ions (m^2·s^{-1}) and D_w its value in water (m^2·s^{-1}), whereas τ and $\vec{\mu}$ refer to the pore tortuosity (-) and the flow velocity (m·s^{-1}).

The Donnan equilibrium model proposed by Birgersson and Karnland (2009) considers only the interlayer porosity to represent interconnected porosity in compacted bentonite, i.e., $\varphi_{tot} = \varphi_{IL}$. The interlayer concentrates most of the positive charge of the system. However, the transport is restricted by the bentonite electroneutrality, which assumes that the interlayer will always retain most of this charge in order to compensate the excessive negative surface charge (see Equation 4-26). This means that a very small charge can be effectively leached, which corresponds to the cations compensating the negative charge of the mobile anions present in the interlayer. Thus, most of the ionic transport will correspond to cation exchange processes with the external water. This retention capacity will also lead to the presence of a concentration jump at the bentonite – water interface, the so-called Donnan equilibrium, specified by a Donnan factor (f_D in Equation 4-27). For modelling this slit boundary condition on the interface, denoted as Γ from now on, Equation 4-24 has been divided in two transport problems defined in the subdomains Ω_b and Ω_f with the concentration variables c_i^{int} and c_i^{ext}, respectively.

$$\sum f_D^{-z_i} \cdot c_i^{ext} \cdot z_i = \frac{CEC \cdot \rho_w}{w \cdot \left(1 \frac{eq}{mol}\right)} \text{ in } \Omega_b \quad \text{Equation 4-26}$$

$$\frac{c_i^{int}}{c_i^{ext}} = f_D^{-z_i} \text{ on } \Gamma \quad \text{Equation 4-27}$$

where z_i is the ion charge (-), CEC is the cation exchange capacity (eq/kg dry clay), w is the water content in the clay (kgw/kg dry clay) and ρ_w is the water density (kg·m^{-3}). The initial Donnan factor is computed numerically with Equation 4-26 using the initial groundwater composition, but then evolves under the effect of glacial water flow. This leads to a problematic non-linearity at the bentonite-fracture interface in Equations 4-26 and 4-27, which locks the system of equations even with accurate initial guesses. For this reason, when performing the temporal discretization with a finite difference scheme, i.e. BDF2, and solving time step n these two equations have been linearized evaluating f_D at the previous time step as follows:

$$\sum c_i^{int}|_n \cdot z_i = \frac{CEC \cdot \rho_w}{w \cdot \left(1 \frac{eq}{mol}\right)} \text{ in } \Omega_b \quad \text{Equation 4-28}$$

$$c_i^{int}|_n = c_i^{ext}|_n \cdot f_D^{-z_i}|_{n-1} \text{ on } \Gamma \quad \text{Equation 4-29}$$

Another important numerical issue is the solution of the set of Equations 4-28 on Γ, where electro-neutrality is precisely crucial so the exchange through the membrane satisfies charge conservation. However, on this boundary the Dirichlet boundary condition in Equation 4-29 is already prescribed, for which it must be enforced as a weak contribution ($+\int q(Q_c^{int}|_n - CEC)d\Gamma$) to the transport Equation 4-24 for $c_i^{int}|_n$, where Q_c^{int} is the positive charge per mass (eq/kg dry clay) and q is a test function (eq/kg dry clay). However, this approach has an important inconvenience: it interferes with the calculation of the Donnan factor in Equation 4-28, leading to a fix value and thus to a stiff equilibrium that does not adapt to the evolving composition of the water outside the buffer. For this reason, an alternative ionic strength constraint has been applied ($+\int w(IS|_n - IS_0|_n)d\Omega_b$) to Equation 4-24 for c_i^{int}, where IS is the total ionic strength in the interlayer and IS_0 is the initial ionic strength of the cations plus that of the mobile anions. This approach has two important effects: it allows compensating nearly all the structural charge (CEC) and it also prevents the ionic strength increasing indefinitely due to the absorption of divalent cations.

$$IS = \frac{1}{2} \sum_i z_i^2 c_i^{int} \quad \text{Equation 4-30}$$

Finally, the transmission condition between the two subdomains must be carefully assessed. Since the finite element method does not satisfy the conservation of fluxes by construction, the flux coming from the buffer must be explicitly prescribed to the exterior (i.e., the fracture domain) transport problem (Codina and Baiges 2011). In COMSOL, the standard natural boundary condition imposition fails in imposing the continuity of fluxes due to the presence of the sharp concentration gradient coming

from the Donnan factor. Therefore, two extra weak contributions corresponding to the conservation of sodium and calcium normal component of the fluxes have been added to Equation 4-24 for c_i^{ext} using Nitsche's method (Juntunen and Stenberg 2009):

$$+\alpha \int w(\Phi_{Na}^{ext}|_n - \Phi_{Na}^{int}|_n)d\Gamma + \beta \int w(\Phi_{Ca}^{ext}|_n - \Phi_{Ca}^{int}|_n)d\Gamma,$$

where α and β are non-dimensional parameters which strengthen the condition but are limited by convergence. In the present case, α = 200 and β = 1 200. The weakly imposed boundary conditions at the bentonite-water interface have only been applied to Na and Ca in order to avoid redundancies with the ionic strength constraint and the Donnan equilibrium, otherwise the system does not converge properly due to an excessive stiffness. The normal component of the fluxes Φ_i^{ext} (mol·m^{-2}·s^{-1}) is defined as follows:

$$\Phi_i^{ext} = \left(-D^{int}\nabla c_i^{int} + \vec{u}^{int} c_i^{int}\right) \cdot \vec{n}^{int}, \qquad \text{Equation 4-31a}$$

$$\vec{n}^{int} = -\vec{n}^{ext}, \qquad \text{Equation 4-31b}$$

where $\vec{n}$ is the normal vector to the buffer-water interface.

5 Numerical models setup

5.1 Bentonite expansion and erosion

The conceptual model described in Chapter 4 is implemented as a three-dimensional (3D) coupled model using COMSOL Multiphysics (COMSOL 2018). This includes two transport equations, one for Na^+ and the other for smectite, as well as a flow equation, which are solved in a staggered fashion.

As shown in Section 4.1, the modelled geometry is a fracture with an aperture varying from 0.1 to 1 mm and an encapsulated bentonite pellet cutting through the fracture. Although the two transport equations and the laminar flow problem do not require a fine spatial discretization of the domain, the geometrical setup and the high initial concentration gradients demand an accurate refinement on the external boundary of the pellet and on the two fracture walls (see Figure 5-1). In the first case, the discretization of the perimeter (of the cylindrical bentonite pellet) has been refined to minimize mass losses during the initial transient, whereas the perpendicular direction has been divided in 7 elements for capturing the viscous boundary layer in the cases with flow. Elsewhere in the fracture plane, the element size has been set to 3 mm, leading to a mesh with a total number of 105k linear finite elements.

The analysed period ranges from 19 to 30 days depending on the simulated test. Temporal discretization is based on the adaptive time stepping of COMSOL according to local error estimators, as well as the integration scheme, which can switch between BDF1 and BDF2 (BDF = Backward Differentiation Formula).

Closed (i.e. zero concentration-gradient) boundary conditions are imposed on all external contours of the model except the seeping water inlet and outlet, where the groundwater flow values and an open boundary are prescribed, respectively.

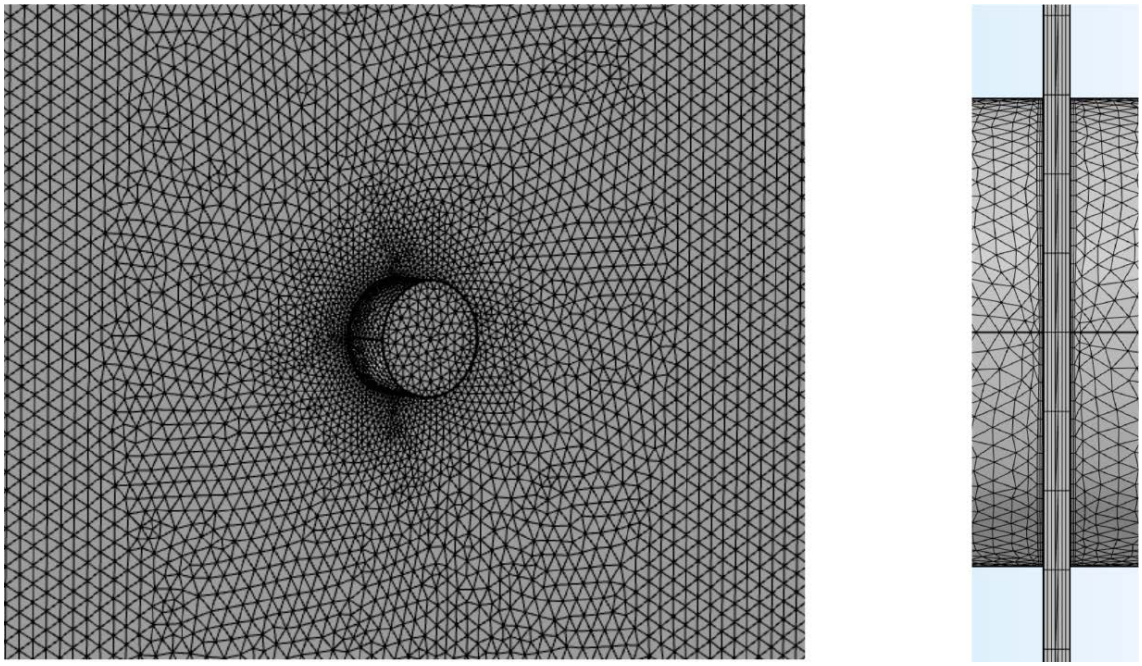

Figure 5-1. *Finite element mesh used in the simulations showing the two refinement processes.*

5.2 Diffusion in the buffer system

The two presented models have been implemented in the finite element computational platform COMSOL Multiphysics (COMSOL 2018) with the reference 3D geometry of the installed buffer (SKB 2011) together with a single horizontal fracture 5.5 × 8 m with an aperture of 0.116 m as shown in Figure 5-2. (Sena et al. 2010) All scenarios (see Table 3-2) have been simulated with the same spatial discretization: 150k linear tetrahedral elements with specific refinement in the fracture (9 elements in the 0.116 m aperture) and on the bentonite – water interface (minimal element size of 65 mm on the fracture plane, see Figure 5-3).

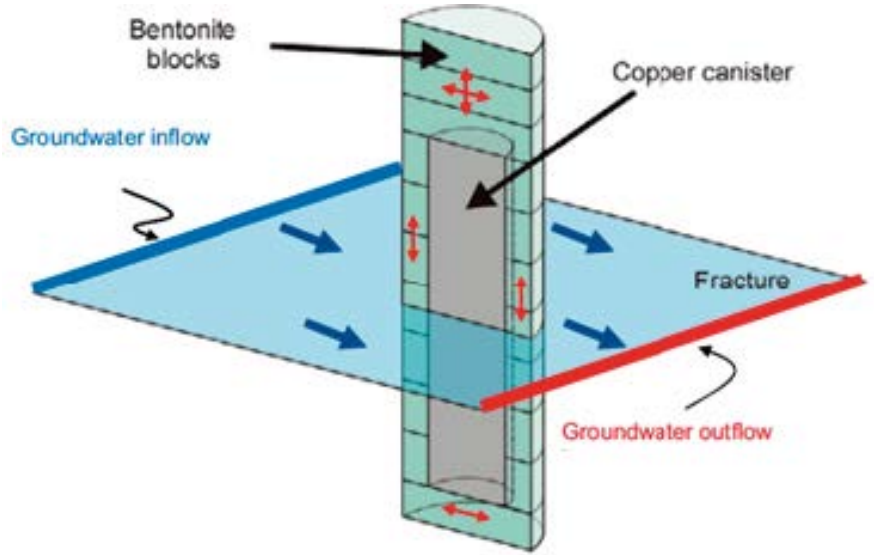

Figure 5-2. *Schematic representation of a horizontal fracture crossing the bentonite buffer (Sena et al. 2010).*

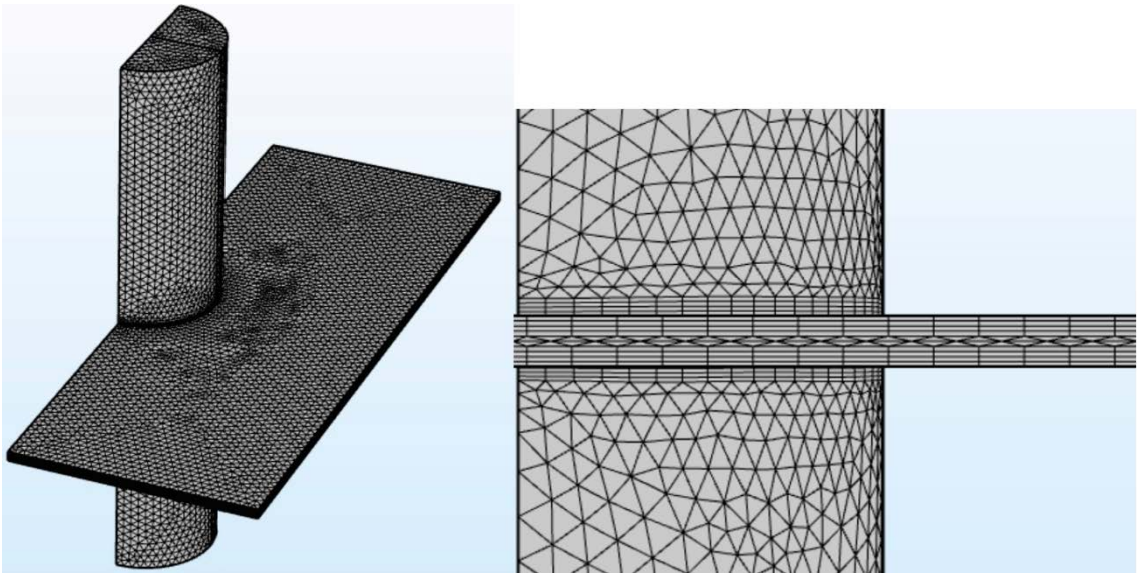

Figure 5-3. *Finite element mesh with boundary layer refinement.*

The initial conditions in the bentonite domain have been obtained with the chemical code PhreeqC (Parkhurst and Appelo 2013) as an equilibrium between MX-80 bentonite porewater (composition calculated with a 40 – 60% mixture with groundwater and equilibrated with the exchanger and accessory minerals) and Forsmark groundwater (Arcos et al. 2006) for the Fickian diffusion model, and by equilibrating the bentonite interlayer water and the same groundwater for the Donnan approach. This calculation has also provided the most relevant ions in the mixture for both cases, each of them to be solved with the corresponding transport equation: Na^+, Ca^{2+}, HCO_3^-, Cl^-, Mg^{2+}, SO_4^{2-}. In the second case, the equilibrium has been recalculated considering only the selected ions in order to provide electroneutral initial conditions (see Table 5-1).

Table 5-1. Initial free porewater concentrations used in the Fickian diffusion models (left), and initial interlayer concentrations used in the Donnan model (right).

Ion	Initial porewater concentration (mM)	Initial interlayer concentration (mM)
Na^+	158.4	539.36
Ca^{2+}	5.209	830.41
HCO_3^-	1.552	0.278
Cl^-	82.74	23.74
Mg^{2+}	2.574	312.10
SO_4^{2-}	61.0	9.60×10^{-3}

Table 5-2. Forsmark groundwater and glacial water compositions.

Ion	Concentration in Forsmark groundwater (mM)	Concentration in Forsmark glacial water (mM)
Na^+	85.71	7.359×10^{-3}
Ca^{2+}	20.97	7.180×10^{-2}
HCO_3^-	1.751	8.515×10^{-2}
Cl^-	149.4	1.410×10^{-2}
Mg^{2+}	7.881	4.114×10^{-3}
SO_4^{2-}	3.797	5.305×10^{-3}

On the other hand, the glacial water composition given in SKB (2010) has been used as inflow boundary condition, whereas Forsmark groundwater (Arcos et al. 2006) has been set as initial condition in the fracture domain in order to avoid a sharp initial transient (see Table 5-2).

A steady precomputed flow field is used for all transport calculations. The fracture size and equivalent water flow range have been obtained from Sena et al. (2010). Five inlet velocity values ranging between 10^{-5} m·yr^{-1} (reference case in SKB 2006) and 0.11 m·yr^{-1} (extreme case, Arcos et al. 2006) have been used to evaluate the effect of this parameter on the solute leaching rate when using the Fickian transport model, which accounts for transport through free porosity (Table 3-2). Regarding the Donnan approach, the study has been restricted to the lowest and highest flowrates (cases C1 and C2).

Since this model does not include the coupling with the smectite transport equation, the corresponding results in Chapter 7 may overestimate the diffusivity of ions through the buffer – fracture interface. According to Neretnieks (1986) and Neretnieks et al. (2010) the presence of clay extrusion in the fracture would have the effect of decreasing the transport rate of ions. Thus, the present models can be considered a pessimistic approach to this phenomenon.

6 Results: bentonite expansion and erosion

6.1 Verification of the implementation for pure expansion

First, the resulting swelling pressure for different salinities is plotted in Figure 6-1 together with experimental measurements from Karnland et al. (2005) corresponding to a Na-homoionized MX80 bentonite, showing a reasonably good agreement in the operational range (i.e. $\rho_d < 1\,500$ kg·m^{-3}). Still, this comparison illustrates the sensitivity that the smectite diffusion equation can have at low densities, considering that the diffusivity depends on the force imbalance giving rise to swelling pressure.

The first simulation corresponds to the verification of the basic implementation in COMSOL of Neretnieks' model without any of the presented extensions. For this purpose, test 11 of Schatz et al. (2013) has been modelled and simulated using the setup described in Section 5.1. This test consists of a pure bentonite expansion test (i.e., with no flow) in a 1 mm fracture filled with deionized water (fracture connected to a reservoir with [Na^+] = 0.03 mM), where wall friction is not expected to significantly limit expansion during the analysed time span (30 days). This allows a double verification with the experimental test and the simulation results provided by Neretnieks et al. (2017) using the same model, as shown in Figure 6-2. This figure summarizes the time evolution of bentonite expansion in the fracture of test 11 as observed experimentally and compared with the modelling results.

The simplified version of Neretnieks' model presented by Schatz et al. (2013), named BESW, has also been evaluated with the setup described in Chapter 5. Although this implementation fits the viscosity and the smectite diffusion coefficient curves leading to a faster convergence, it tends to overestimate expansion quite significantly (Figure 6-2). In fact, the fitting of the diffusion coefficient in Schatz et al. (2013) shows a considerable error at the low smectite concentration range for [Na^+] > 0.1 mM. Since the main goal of the project consists in developing a numerical tool for general use, this implementation has not been further used in this work.

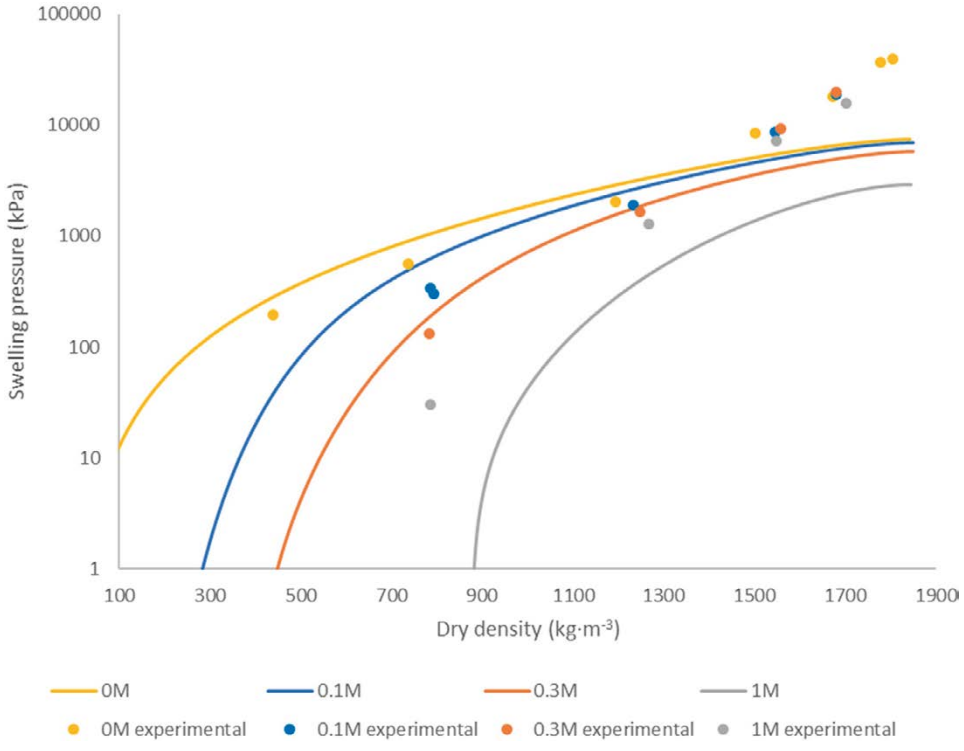

Figure 6-1. *Swelling pressure calculated with Neretnieks' model (straight lines) and experimental data (dots) from Karnland et al. (2005).*

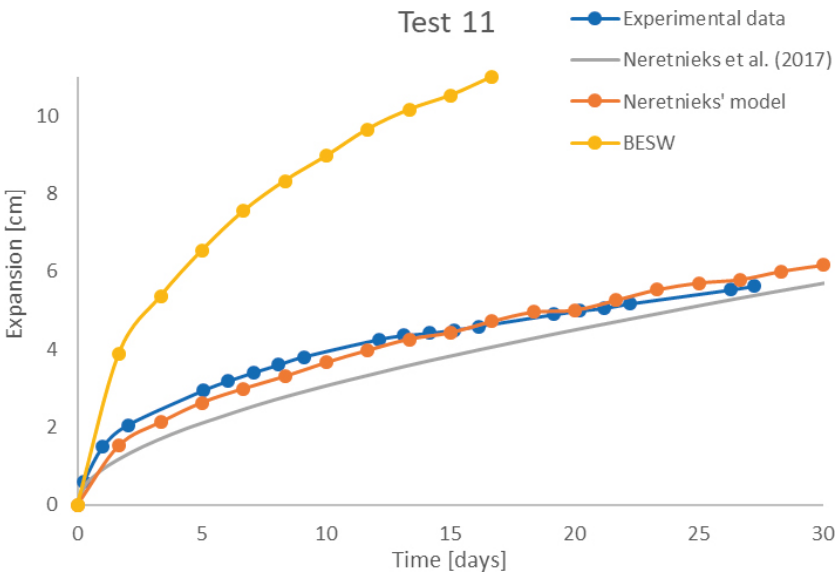

Figure 6-2. *Time evolution of bentonite expansion during 30 days: experimental data (test 11 in Schatz et al. 2013) and numerical modelling results from Neretnieks et al. (2017) using Neretnieks's model, and for Neretnieks's model and BESW (Schatz et al. 2013) both implemented in the current study for the setup described in Chapter 5.*

The model results using Neretnieks's model agree reasonably well with the experimental results and the results obtained by Neretnieks et al. (2017). The model reproduces both the rate and the absolute values of expansion. Still, there are some differences with the results previously obtained in Neretnieks et al. (2017), although these could be attributed to the different setups: model geometry (3D instead of 2D), spatial and temporal discretization, and where the smectite expansion equation is solved (in this work over the entire model domain, including the bentonite pellet).

6.2 Preliminary analysis of bentonite erosion

Although the main objective of the present report consists in providing a numerical model for bentonite expansion in low salinity fracture waters, the ultimate goal of the POSKBAR project is the quantification of bentonite erosion. At this stage, several aspects are still to be analyzed and implemented in the model, but a preliminary assessment has been performed to identify the current disagreements between experimental and model results. For this purpose, test 3 of Schatz et al. (2013) with a duration of 19 days has been selected as reference case because it combines the configuration of the test 11 with a high fracture flowrate (2×10^{-4} m·s^{-1}).

As stated in Chapter 4, Neretnieks' model with Darcy's law strongly underestimates erosion (Neretnieks et al. 2017). This fact can be observed in the amount of eroded bentonite in test 3 shown in Table 6-1. In the case of the two-region model presented by Neretnieks et al. (2017), the calculation of a second transport problem at the rim region manages to capture the interaction between seeping water and sol but overestimates the mass losses. This disagreement might have to do with the need for calibration and the lack of coupling with the flow equations.

In order to evaluate the error introduced by the permeability models described in Section 4.3.1 in the computation of smectite erosion, test 3 has been simulated with both Brinkman and Stokes equations. As expected, due to the strong permeability decrease in the sol region (Figure 4-2) the Brinkman equations with the Kozeny-Carman model (KC) and the modified Kozeny-Carman correlation (MKC) provide similar results to those obtained with Neretnieks' model using Darcy's law. In contrast, the viscosity-scaled permeability (Brinkman equations) and the Stokes equations, the latter relying only on the shear resistance to withstand erosion, provide an excessive mass loss (see Table 6-1). However, this last case provides a worst-case scenario without resorting to empirical models.

Table 6-1. Eroded bentonite mass (g) in test 3 after 19 days. References: [1] Schatz et al. (2013); [2] Neretnieks et al. (2017); [3] Moreno et al. (2010).

Experimental	Neretnieks' model	Two-region model	Brinkman (KC)	Brinkman (MKC)	Brinkman (viscosity)	Stokes
[1]	[2]	[2]			[3]	
4.7	0.33–1.74	5.74–10	0.92	1.1	8	9

Another important aspect analyzed in Chapter 4 is the equilibrium between expansion and erosion rates. Pseudo-steady state conditions can even be found in extreme scenarios with a high flow rate and deionized water as in test 3 (for as long as the bentonite source can be considered constant). In this sense, Table 6-2 shows both experimental and simulated radial expansion using either Brinkman or Stokes equations for solving the flow. Whereas Brinkman equations with KC and MKC reproduce similar results to those obtained in test 11 (little erosion), Stokes equation predicts a very limited expansion (Table 6-2), due to an excessive erosion rate (see Figures 6-3 and 6-4). In-between, the Brinkman equations with the viscosity-scaled permeability (Moreno et al. 2010), yields the best approximation, but does not manage to reproduce a realistic equilibrium between erosion and expansion either.

Table 6-2. Comparison of bentonite radial expansion after 19 days (test 3of Schatz et al. 2013); experimental measurement and model results using either Brinkman or Stokes equations.

	Radial expansion (cm)
Experimental	2.3
Flow model version	
Brinkman (KC)	6 (non-steady)
Brinkman (MKC)	5 (non-steady)
Brinkman (viscosity-scaled)	0.67
Stokes	0.3

Therefore, it can be concluded that Equation 4-6 (Stokes equations accounting for swelling pressure) should be used for two reasons: to introduce an expansive inertial force that can balance erosion, and to enable the consideration of a non-Newtonian Herschel-Bulkley fluid model for better describing the shear stress that leads to erosion.

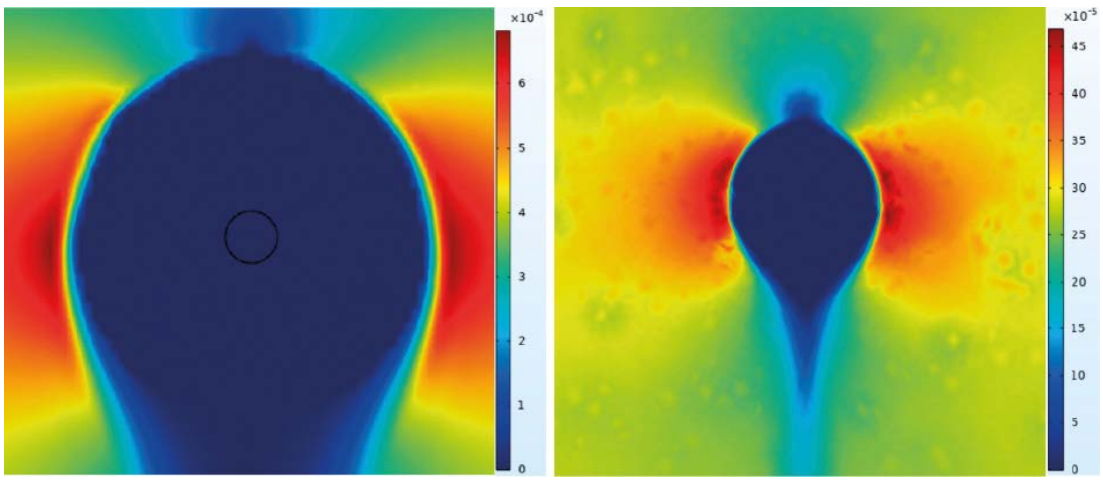

Figure 6-3. *Calculated flow velocity magnitude $|\vec{u}|$ $(m \cdot s^{-1})$ after 19 days (test 3 of Schatz et al. 2013), using Brinkman equations with modified Kozeny-Carman (left) and Stokes equations (right).*

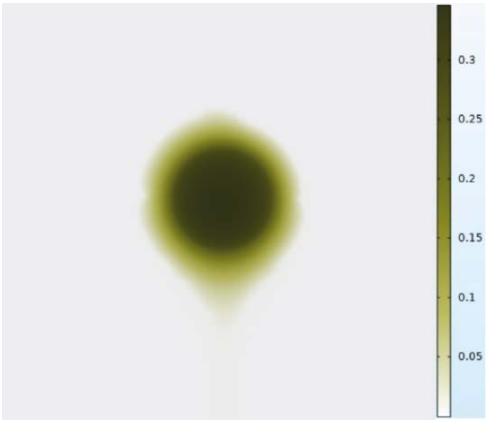

Figure 6-4. *Calculated radial expansion of bentonite volume fraction (φ) in test 3 of Schatz et al. (2013) with Stokes equations. Note the presence of a bentonite tail downstream (flow from top to bottom).*

6.3 Quantification of bentonite expansion

Preliminary simulations of bentonite expansion with the proposed model, which includes the effect of solid friction (Åkesson et al. 2010), shear stress and interfacial tension with stagnant water, have revealed a significant sensitivity with the fracture aperture. Thus, the same test case with fracture apertures of 0.1, 0.2, 0.4 and 1 mm has been modelled. They correspond to tests 4B, 6B, 8A and 52A of Alonso et al. (2019), respectively. These tests were performed with Nanocor commercial Na-exchanged and purified montmorillonite with an initial dry density of 1 400 kg·m^{-3}. The test setup considers an initial sodium concentration in groundwater of c_w = 1 mM, a porewater concentration of c_b = 750 mM, and no external flow. Thus, only Equations 4-16 and 4-21 are solved. Each test has been simulated twice for quantifying the effect of the wall friction advective term (version 1 – without, version 2 – with wall friction and surface tension effects). The final state measured experimentally after 30 days regarding bentonite expansion and water electrical conductivity of the four selected tests is summarized and compared to model results in Table 6-3. Electrical conductivity is obtained from Na concentration (1 mM corresponds to 100 μS/cm).

Table 6-3. Bentonite expansion and water electrical conductivity (E.C.) for the four selected tests in Alonso et al. (2019) after 30 days. Model and experimental results.

Test	Fracture width (mm)	Version	Radial expansion (cm)	Water final E.C. (μS/cm)
4B	0.1	Experimental Model v1 Model v2	1.29 2.69* 1.31	6 260 2 189 3 338
6B	0.2	Experimental Model v1 Model v2	2.5 2.55* 1.51	n.d. 2 169 3 251
8A	0.4	Experimental Model v1 Model v2	2.26 2.30* 2.42	1 315 3 168 3 395
52A	1.0	Experimental Model v1 Model v2	2.7* 1.86* 2.89*	3 170 2 015 4 184

* No steady state reached

In this case, unlike test 11 of Section 6.2, some simulations reach steady state (4B, 6B), while model 8A is about to do so. On the other hand, model 52A (largest aperture) does not seem to stop after 30 days. Although water chemistry can be partly responsible for that (the system is closed and water is not cleaned), a clear dependency on δ can be observed in Figure 6-5. Therefore, we can conclude that bentonite – fracture contact shear forces play an important role in compensating the swelling

capacity. In this scenario, Neretnieks' model cannot provide the required mechanical equilibrium and, as expected, does not reach steady state in any of the modelled cases (see Table 6-3 and Figure 6-5).

The calculated electrical conductivity of the solution in the fracture after 30 days is also compared to the experimental one to analyze the possible error resulting from the simplification of the chemistry and solute transport. This could have a non-negligible impact on the bentonite swelling capacity. In this sense, Table 6-3 shows a clear disagreement for most of the cases, although the calculated values lay within the same order of magnitude of the corresponding measurements performed by Alonso et al. (2019), for which the impact of salinity on the modelled expansion is expected to be rather moderate.

It must be noted that $\dot{\gamma}_0$ in Equation 4-10 has been defined as $\dot{\gamma}_0 = v_0\delta^{-1}$, with $v_0 = 5 \times 10^{-8}$ m·s^{-1}, which is approximately equal to the initial diffusive flux $\chi f^{-1} \nabla\varphi$ (m·s^{-1}) that leads to mobilization. As stated in Chapter 4, this assumption is only a first approximation that should be replaced in a future stage by the strain rate computed with Equation 4-7. This configuration leads to a good adjustment of the expansion evolution for case 4B, managing to reproduce the early retention observed for $\delta = 0.1$ mm (see Figure 6-6), whereas the wall friction effect for case 6B ($\delta = 0.2$ mm) is significantly overestimated (see Figure 6-5). No experimental data regarding water final ionic strength is provided for test 6B. Therefore, the notable difference between the measured expansion in cases 4B and 6B might not be totally related to the confinement degree, but solute concentration could also play a role. On the other hand, the advective term in Equation 4-16 begins to balance expansion just before the 30 days in case 8A but is not able to do so for case 52A, which does not reach steady state in the experiment either. Another important feature is that both cases expand more than when computed without the wall friction and shear term, which a priori does not make sense. However, Figures 6-7 and 6-8 show how the method succeeds in blocking the expansion of high smectite concentrations, leading to segregation between gel and sol, which allows the latter to expand more than in the previous two cases due to the harsh decrease of the outer interfacial force. As noted in Section 4.4.1, this force, which is inversely proportional to the fracture aperture, is subject to high uncertainties (Jańczuk et al. 1996) in liquid-liquid interfaces and the difference between water and sol surface tensions has been taken as a first guess. For this reason, its quantification should be further investigated. It must also be noted that the calculation of $\dot{\gamma}$ and η_{eff} should be further refined, i.e. coupling the flow equations. However, within the validity range $\varphi < 0.1$ of the rheological model (Pujala 2014), the model has proven to describe quite properly the effect of wall friction and shear resistance on the expansion of smectite.

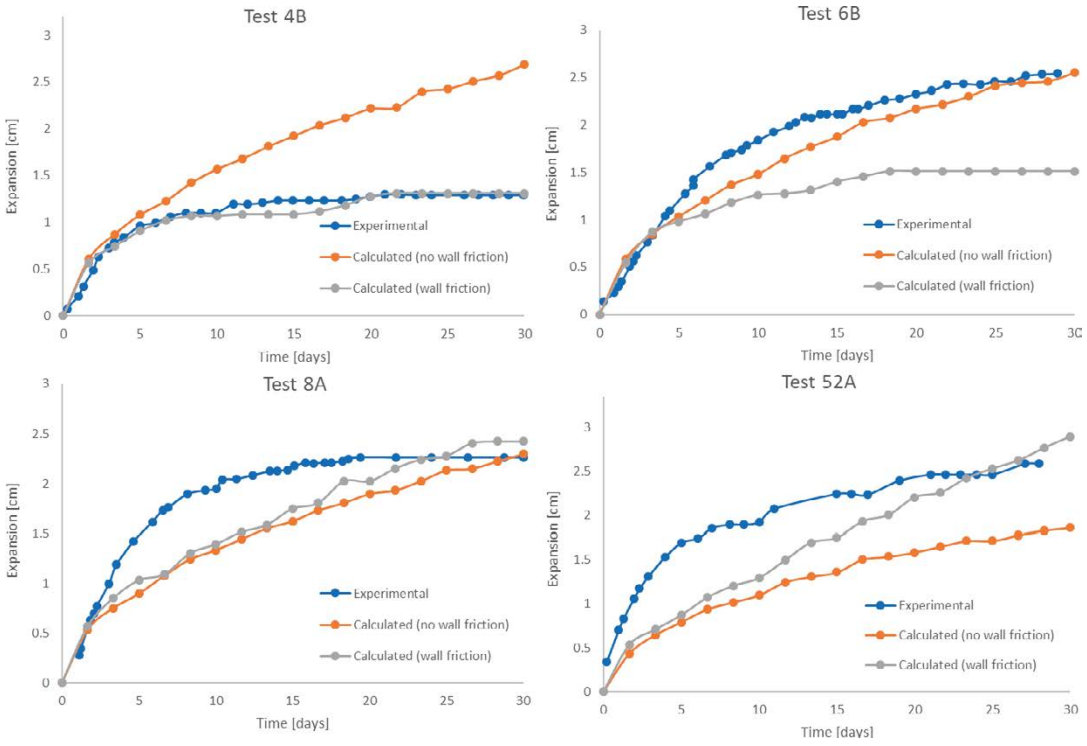

Figure 6-5. *Time evolution of expansion of bentonite volume fraction (φ) in the four selected tests: 4B, 6B, 8A, and 52A (0.1, 0.2, 0.4 and 1.0 mm, respectively). Experimental (from Alonso et al. 2019) and modelling results (with and without wall friction).*

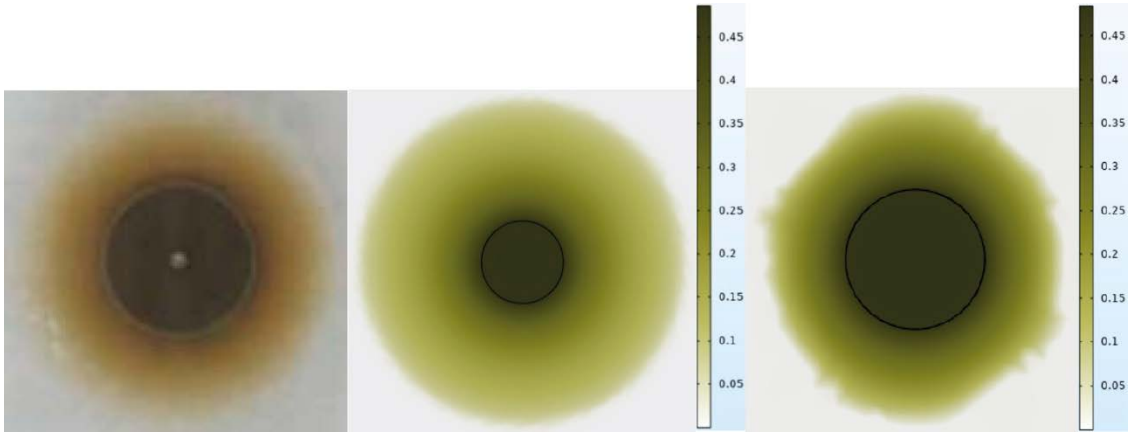

Figure 6-6. *Photograph of the final expansion obtained experimentally in test 4B (δ = 0.1 mm) after 30 days taken from Alonso et al. (2019) (left), volume fraction (φ) profile simulated without wall friction or shear (center) and with wall friction and shear also after 30 days (right). A slight asymmetry is obtained in the model due to the use of a non-radial mesh.*

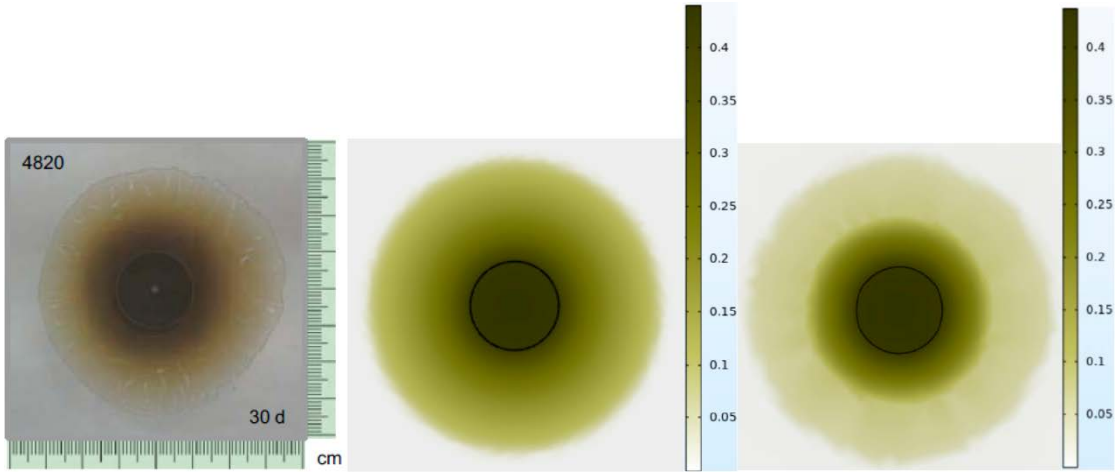

Figure 6-7. *Photograph of the final expansion obtained experimentally in test 8A (δ = 0.2 mm) after 30 days taken from Alonso et al. (2019) (left), volume fraction (φ) profile simulated without wall friction or shear (center) and with wall friction and shear also after 30 days (right). A slight asymmetry is obtained in the model due to the use of a non-radial mesh.*

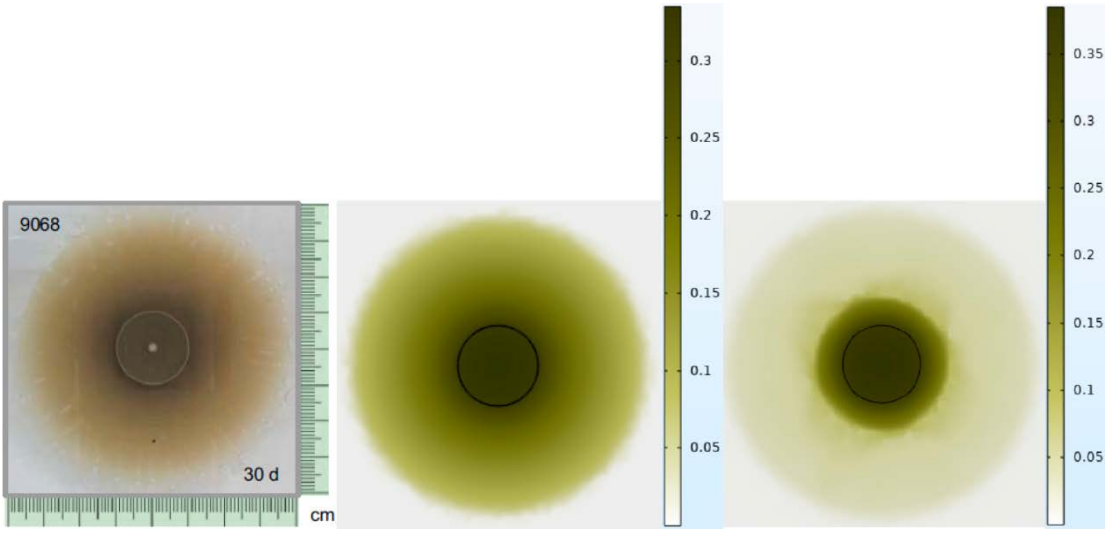

Figure 6-8. *Photograph of the final expansion obtained experimentally in test 52A (δ = 1 mm) after 30 days taken from Alonso et al. (2019) (left), volume fraction (φ) profile simulated without wall friction or shear (center) and with wall friction and shear also after 30 days (right). A slight asymmetry is obtained in the model due to the use of a non-radial mesh.*

7 Results: ionic transport in the buffer under glacial water

7.1 Free porosity Fickian transport

The transport of solutes in the bentonite free porosity, presented in Section 4.5.1 as a simplification of the Multi-porosity approach (Appelo 2013), has been tested for two reasons: first, in order to investigate the early leaching of salts observed in experimental tests by Muurinen and Lehikoinen (1999) and Alonso et al. (2019), and in second place, for providing a worst case scenario in the long-term safety assessment of the KBS-3V concept.

The high solute concentration gradient between the bentonite porewater and the intruding glacial water flow will lead to a significant leaching rate, especially in this extreme case where cation exchange reactions are not considered. The only retention capacity comes from the available porosity itself, which according to the Multi-porosity approach, is restricted by the presence of the interlayer volume fraction and the diffuse double layer (DDL) porosity. Whereas the first one can be considered constant under water saturated conditions, the second one shows a strong inverse dependence on the ionic strength. Thus, under low salinity conditions (low ionic strength), the available free porosity decreases. In order to avoid a highly nonlinear calculation, ten scenarios with extreme values of φ_{free} have been simulated: cases A1-A5 with $\varphi_{free} = 0.11$, which corresponds to the initial saline conditions (Idiart and Coene 2019), and cases B1-B5 with $\varphi_{free} = 0.011$, which accounts for the free porosity reduction due to DDL growth under glacial water intrusion. The exact value cannot be derived with the Multi-porosity model because it yields negative values when assuming glacial water concentrations. This sensitivity study has been combined with the glacial water flow rate variation described in Section 5.2. For the sake of clarity, only the results corresponding to the four extreme cases (A1, B1, A5, B5 in Table 3-2) are shown explicitly below. Results corresponding to the other six cases are summarized in Figure 7-1, which shows the time when CCC is reached in all scenarios.

Despite a much higher free porosity, the first case (shown in Figures 7-2 and 7-4) turns out to be less prone to bentonite erosion than the second one under the presence of a glacial water flow, in the sense that it takes longer to leach the dissolved salts. The harsh reduction of the effective diffusion coefficient leads to an internal concentration gradient in the bentonite as diffusion is not able to compensate the losses caused by flow advection at the fracture interface (compare Figure 7-3 with Figure 7-6). For this reason, case B5 shows a faster ionic strength decrease near the bentonite – water interface (10 cm on the narrowest fracture section, now on buffer midsection) up to CCC (see Figure 7-7) when the dissolved salts in the buffer have not yet been leached (see the gradient along the bentonite column in Figure 7-5). This result shows the importance of the fracture flow conditions, since they can trigger an early degradation of the buffer no matter the solute concentration in the bulk.

According to Birgersson et al. (2009), the CCC is found at 4mM ionic strength for mixed sodium and calcium clays. Figure 7-1 shows the time when this threshold is reached, ranging from 90 years in case B5 to 3 000 years in case A1.

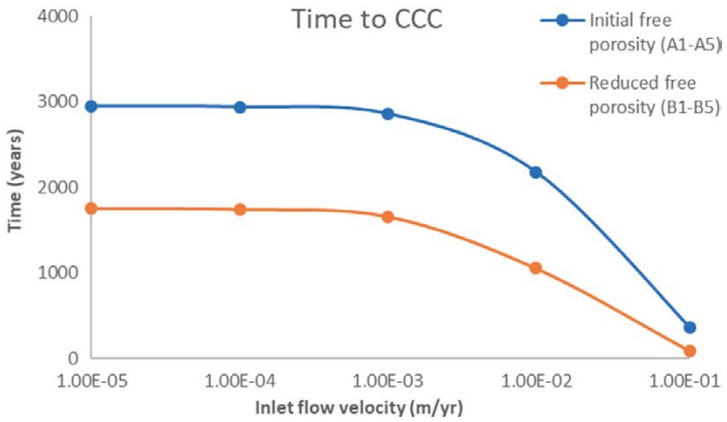

Figure 7-1. *Time to CCC dependence on inlet fracture flow velocity measured at a point located 10 cm away from the buffer on the midsection.*

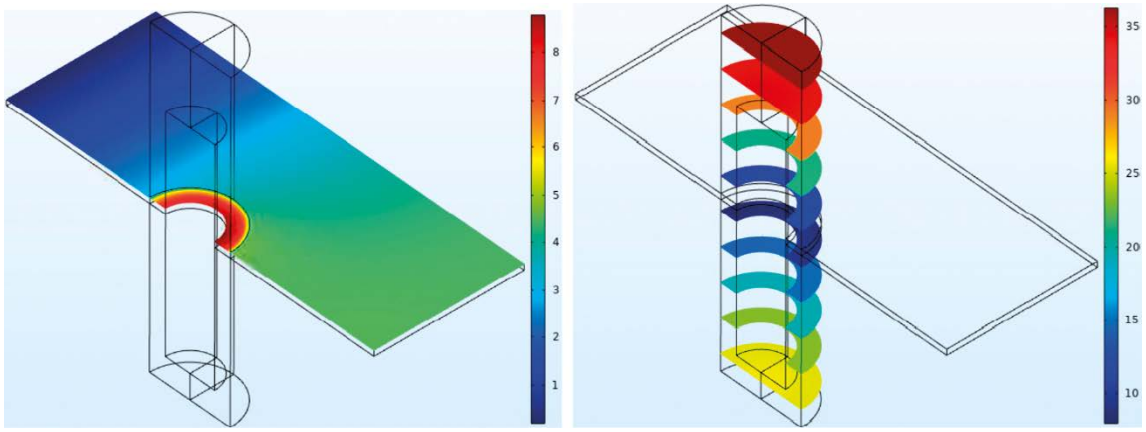

Figure 7-2. *Ionic strength (mM) at the fracture plane (left), in the bentonite buffer (right) when reaching CCC at t = 3 000 years for case A1 (lowest flowrate and* φ_{free} = 0.11*).*

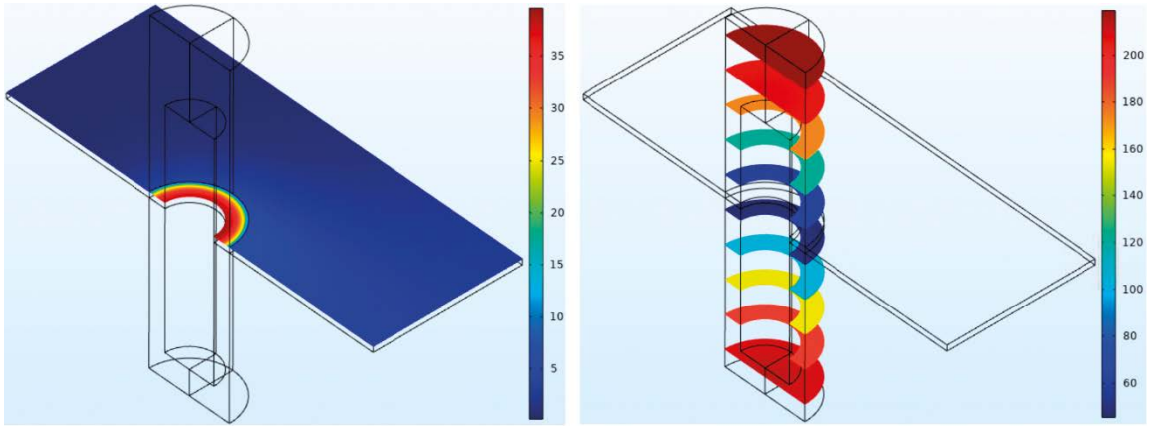

Figure 7-3. *Ionic strength (mM) at the fracture plane (left) and in the bentonite buffer (right) when reaching CCC at t =400 years for case A5 (highest flowrate and* φ_{free} = 0.11*).*

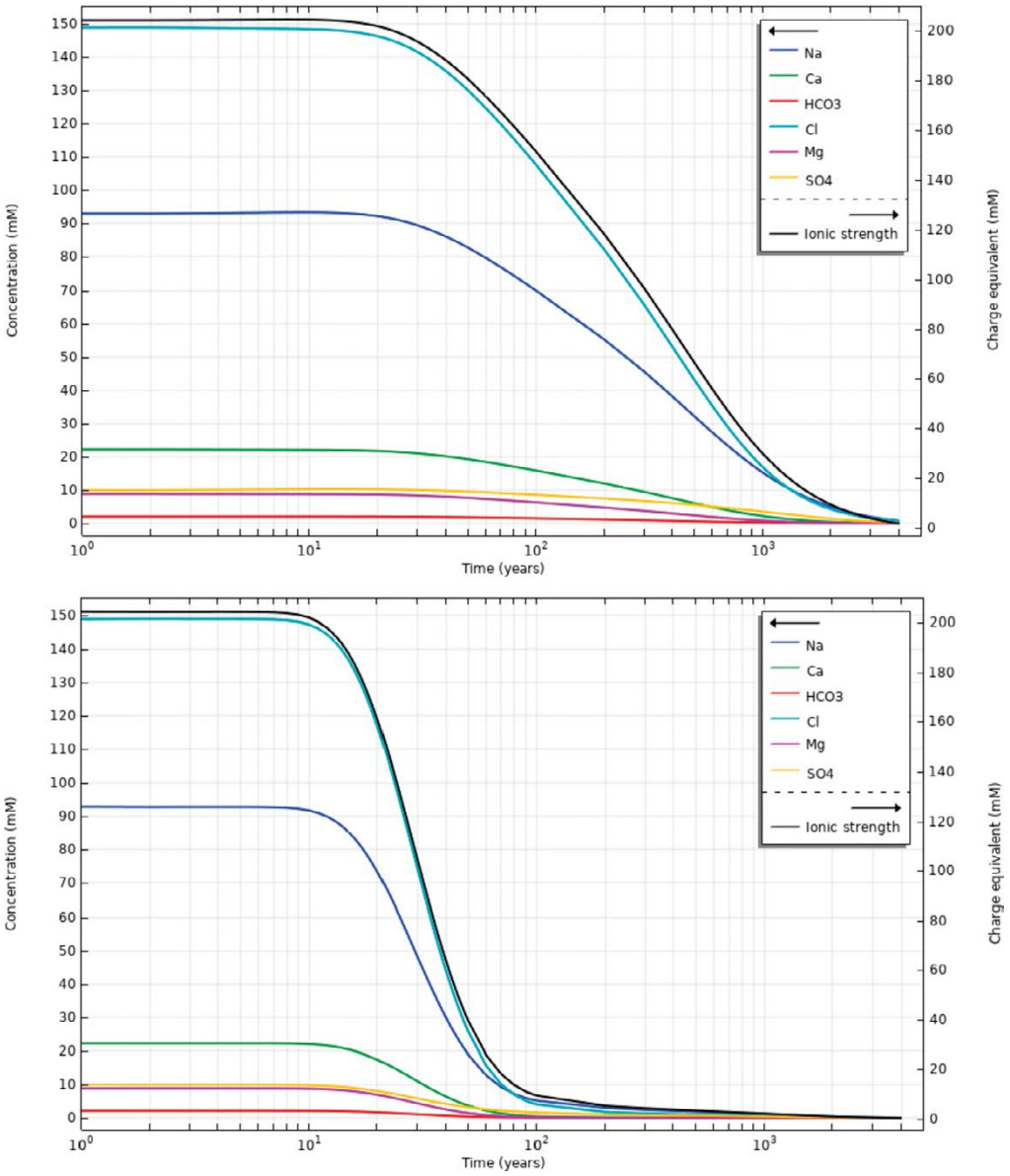

Figure 7-4. *Ion concentrations (mM) and ionic strength (mM) time evolution for case A1 (top) and A5 (bottom) at a point located 10 cm away from the buffer on the midsection.*

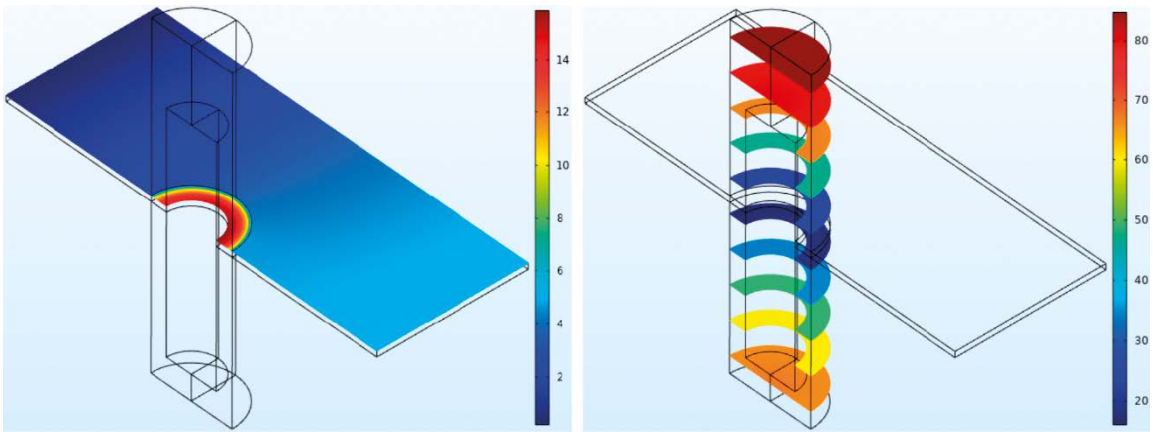

Figure 7-5. *Ionic strength (mM) at the fracture plane (left) and in the bentonite buffer (right) when reaching CCC at t = 1 800 k years for case B1 (lowest flowrate and φ_{free} = 0.011).*

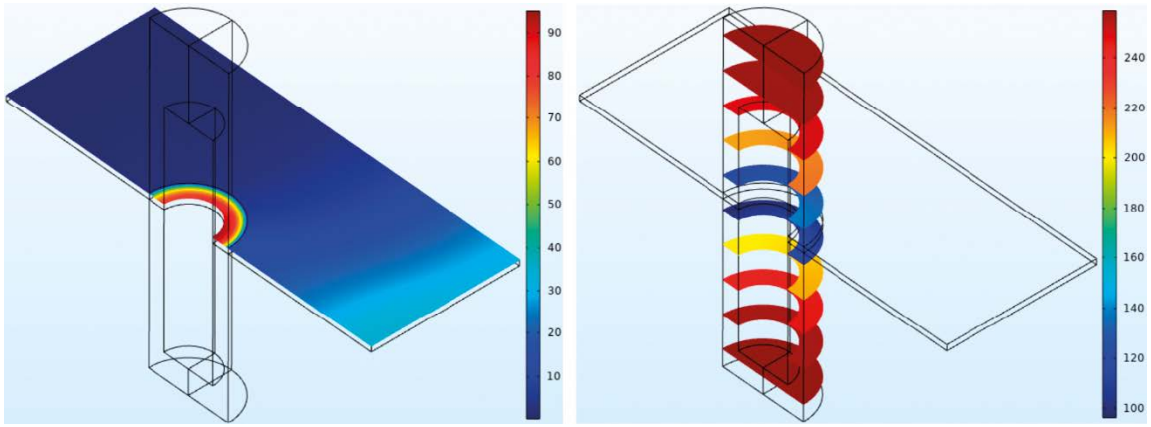

Figure 7-6. *Ionic strength (mM) at the fracture plane (left) and in the bentonite buffer (right) when reaching CCC at t = 90 years for case B5 (highest flowrate and* φ_{free} = 0.011*).*

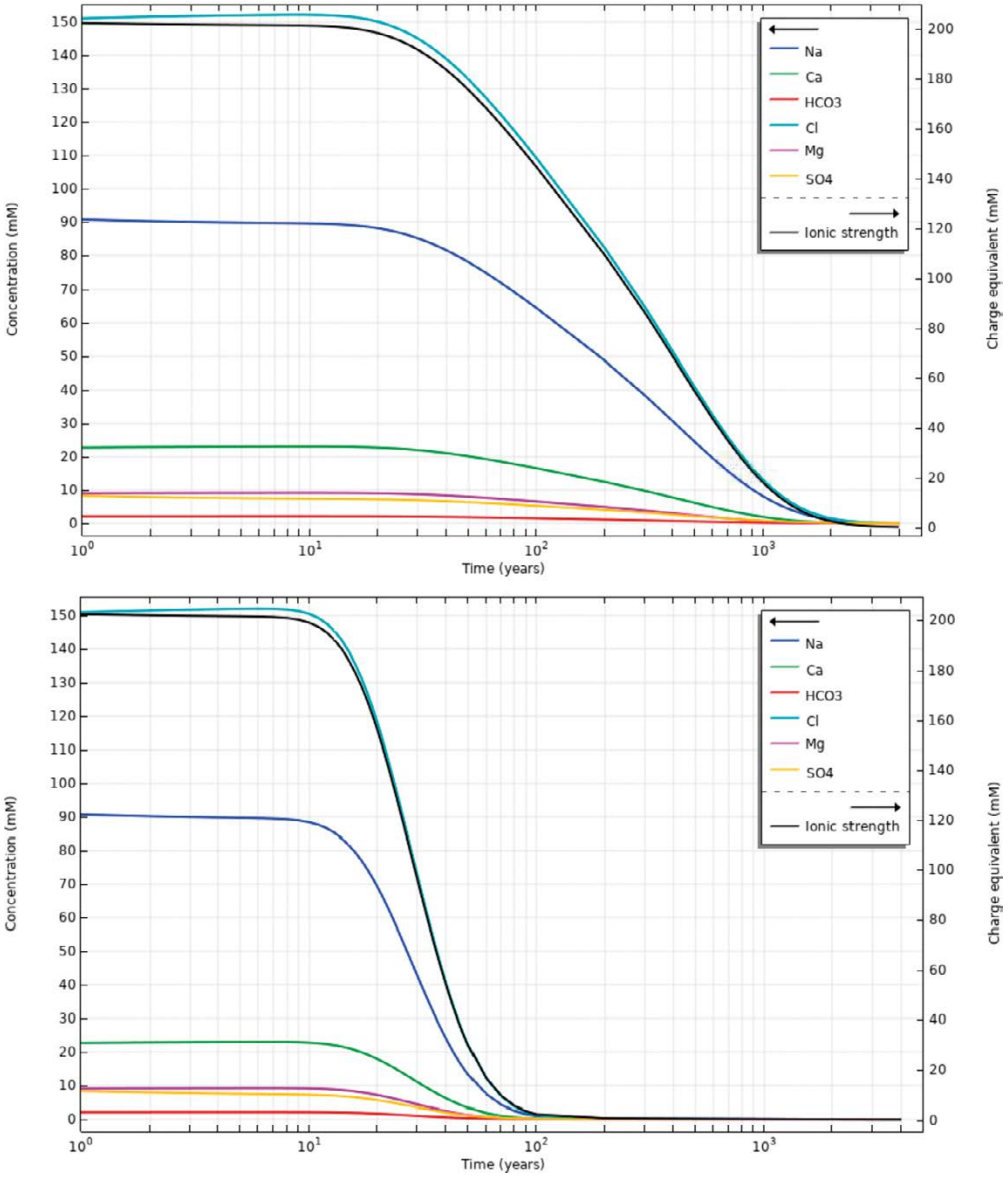

Figure 7-7. *Ion concentrations (mM) and ionic strength (mM) time evolution for case B1 (top) and B5 (bottom) at a point located 10 cm away from the buffer on the midsection of the buffer.*

7.2 Donnan model

Unlike the previous approach, the Donnan model (Birgersson and Karnland 2009) enforces electro-neutrality in the bentonite interlayer water. This means that cations will always compensate the bentonite structural negative charge, plus the small concentration of mobile anions that could enter the interlayer. Thus, only a very small fraction will be leached to the fracture in this case. Instead, the loss of sodium is driven by exchange processes with other cations, mainly calcium and magnesium in the presence of glacial water. This leads to a higher retention capacity, even in highly advective scenarios, with a less concentrated but more durable plume around the buffer, for which it can be considered a much more optimistic approach than Fickian diffusion. In the present case, the study has been restricted to the lowest and the highest flow rate scenarios (SKB 2006 and Arcos et al. 2006, respectively).

Figures 7-8 and 7-9 show how the Donnan model leads to a retardation of the solute leaching through the fracture after 7 000 years for case C1 and 1 500 years for case C2, when the water at the vicinity of the buffer reaches CCC. The vertical concentration gradients in the bentonite buffer is very small due to the retention capacity of the clay in front of the external advection. For this reason, the leaching rate is smaller than in the Fickian approach (see Figure 7-10). Unlike the Fickian approach, the ionic strength does not tend to zero, but shows the presence of a remnant due to the Donnan equilibrium (see Figures 7-4 and 7-10). Therefore, the disaggregation of the buffer once CCC has been reached is expected to be more critical in the former than in the latter. Magnesium, and calcium to a lesser extent, enter the interlayer at the expense of sodium leaching (see Figure 7-11). This exchange is limited by the total ionic strength restriction in the buffer (Equation 4-30).

Another important outcome of this simulation is the Donnan factor evolution (f_D in Equation 4-27), shown in Figure 7-12. As expected from Equation 4-26, it evolves with the ionic strength at the interface. The Donnan factor corresponding to the equilibrium between the initial bentonite interlayer and the glacial waters is 1.46×10^{-2}. Although this value cannot be reached because of the buffer composition change, the Donnan factor is already 2×10^{-2} when CCC is reached, which shows the significant washing performed by the glacial water at the considered flowrates.

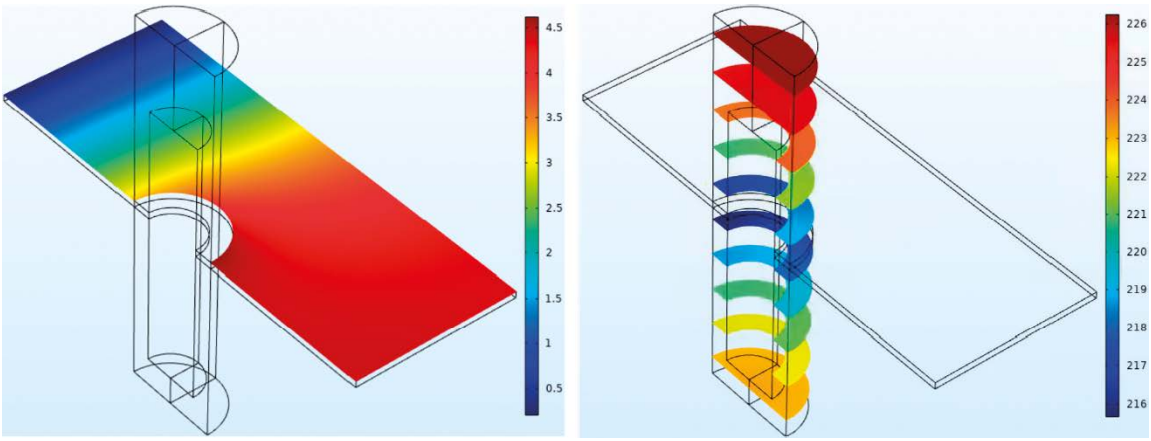

Figure 7-8. *Ionic strength (mM) at the fracture plane (left) and sodium concentration in the bentonite buffer (right) at t = 7 000 years for case C1.*

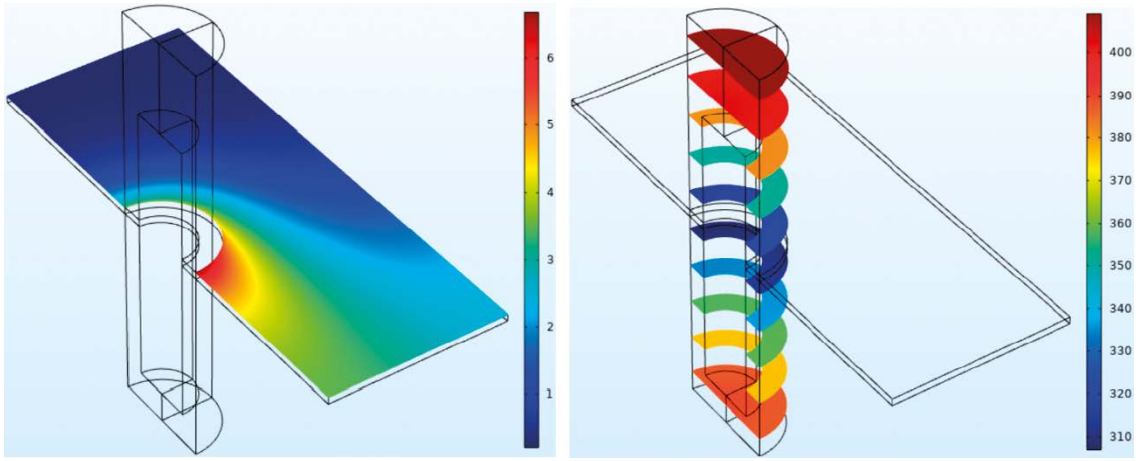

Figure 7-9. *Ionic strength (mM) at the fracture plane (left) and sodium concentration in the bentonite buffer (right) at t = 1 500 years for case C2.*

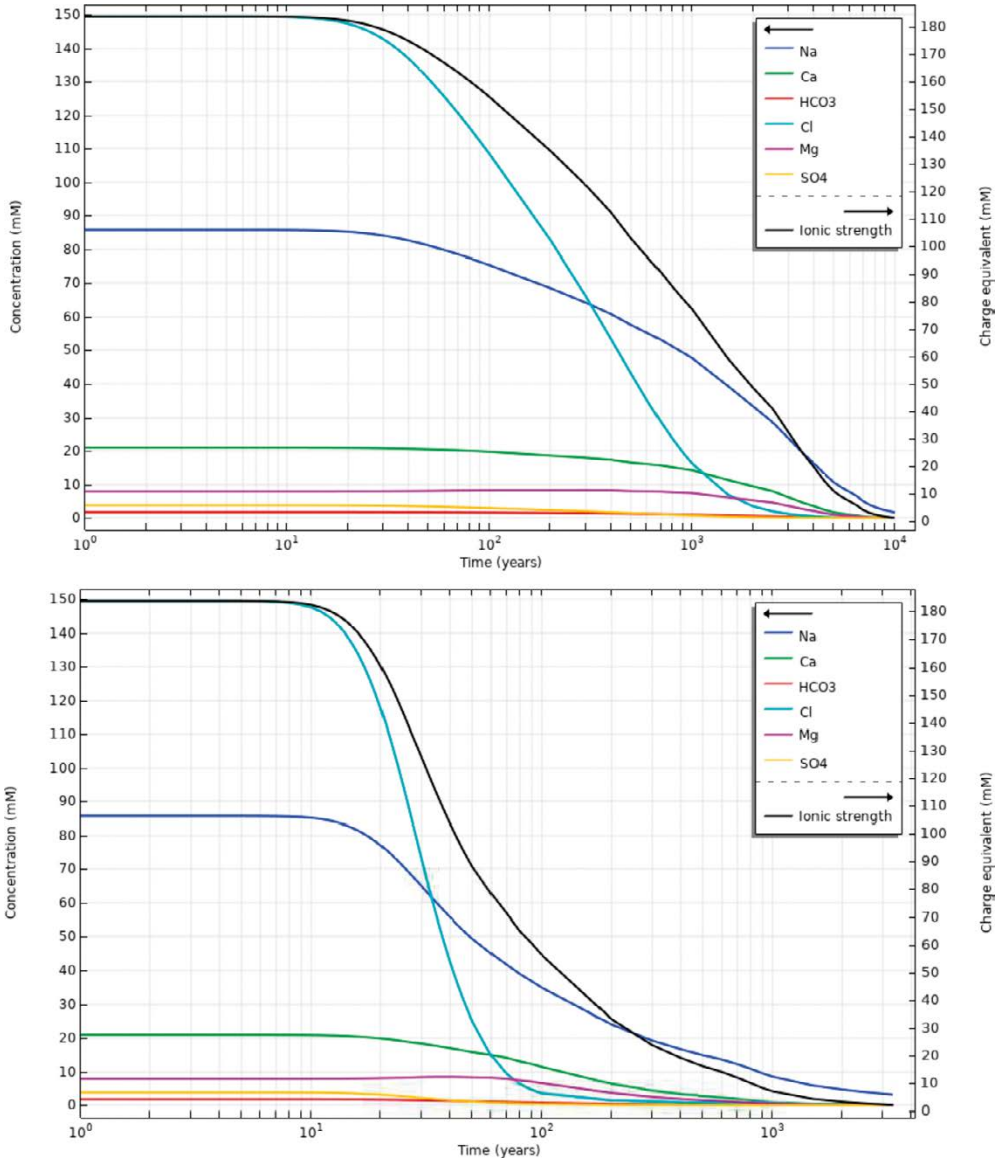

Figure 7-10. *Ion concentrations and ionic strength time evolution for case C1 (top) and C2 (bottom) at a point located 10 cm away of the buffer on the midsection.*

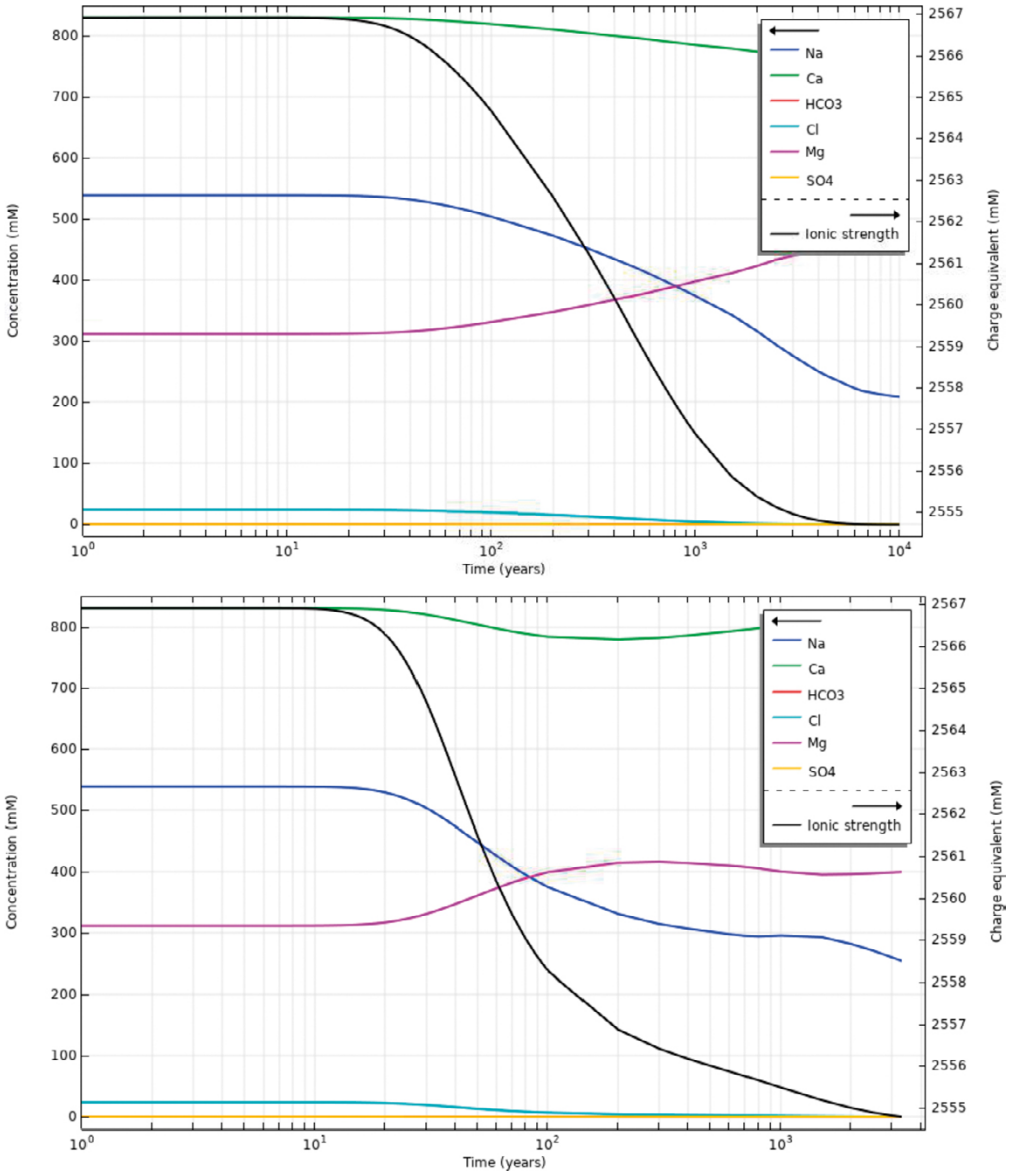

Figure 7-11. *Ion concentrations and ionic strength time evolution for case C1 (top) and C2 (bottom) at a point located 20 cm inside the buffer on the fracture plane.*

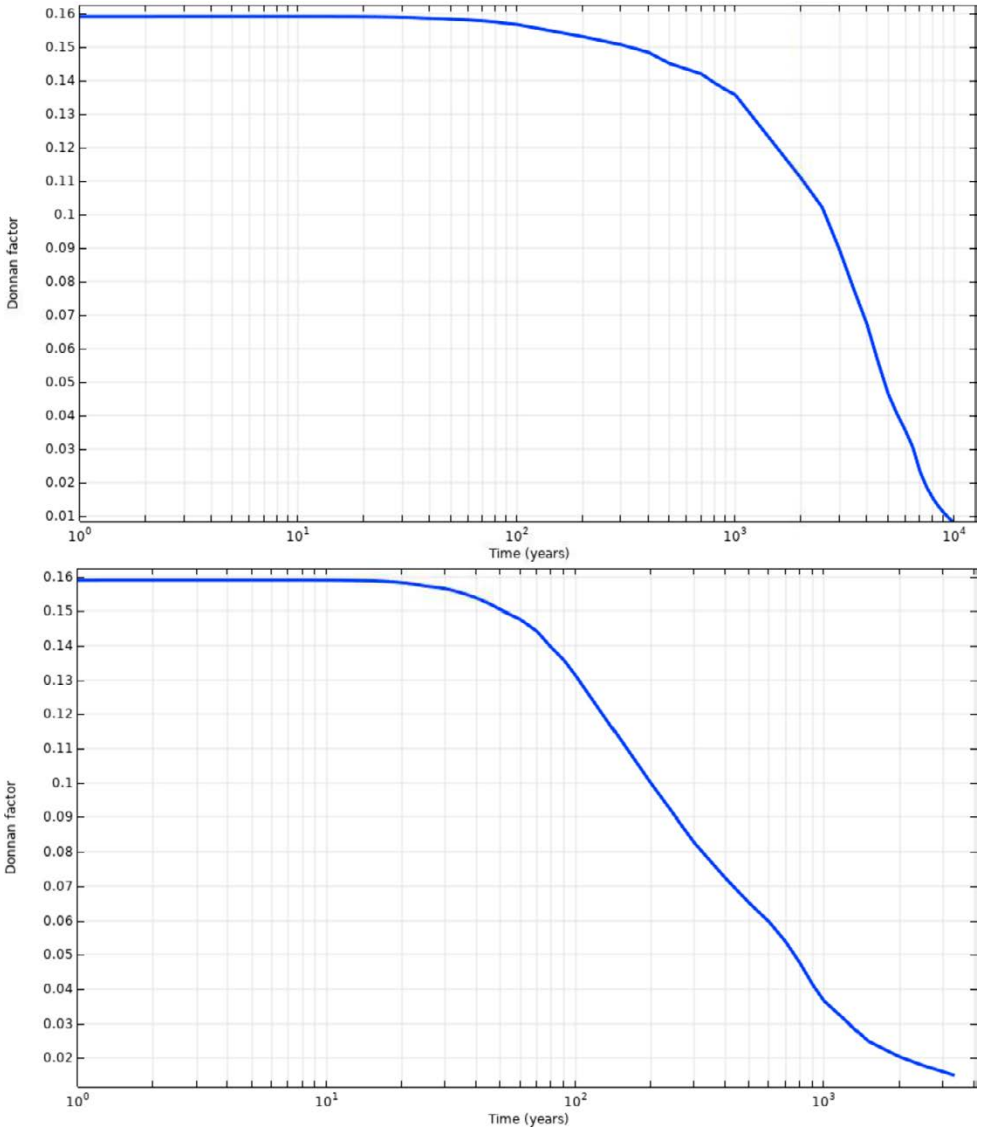

Figure 7-12. *Time evolution of the average Donnan factor (f_D) for case C1 (top) and C2 (bottom).*

8 Discussion, conclusions and future work

8.1 Discussion and conclusions

An extension to Neretnieks' model including the flow equations and the smectite expansion equation (Liu et al. 2009) has been proposed to reduce the disagreements between numerical models and experimental results in terms of bentonite expansion and erosion. At this first stage of the study, the flow and smectite transport equations have been extended with explicit consideration of wall friction and shear resistance.

The first step consisted in the implementation of two different versions of Neretnieks' model in COMSOL: the original one described in Moreno et al. (2010) and the BESW simplified implementation by Schatz et al. (2013). Verification of the models has shown the unsuitability of the latter due to significant overestimation of the diffusivity for a wide range of sodium concentrations, leading to an excessive expansion. Schatz et al. (2013) also reported excessive erosion when simulating some of tests. For instance, their model results of test 3 (same test analysed here in Section 6.2) predict almost full erosion of the entire bentonite pellet mass, which is far from experimental observations.

Given the disagreements between experimental results of swelling expansion in fractures (Alonso et al. 2019) and Neretnieks' model (Neretnieks et al. 2017), a modification of that model accounting for alternative physical processes, such as fluid mechanics and surface tension effects has been formulated. At this first stage, the smectite expansion equation has been extended with a conservative advective term corresponding to the average shear stress due to wall friction of a viscous laminar flow between two plates. This introduces a resistance to diffusion that allows reaching bounded expansion even in the presence of stagnant waters below CCC. With this model, some of the experiments in Alonso et al. (2019) using Nanocor with several fracture apertures have been modelled. Some of the modelled experiments are properly reproduced, although further research in the rheological model is needed for a better quantification of the strain rate. However, the restriction of the model to $\varphi < 0.1$ has proved to be a correct assumption in the sense that high concentration regions do not propagate as much as light gels and sols, for which the effect of wall friction and shear becomes more significant. Moreover, the range of validity of the rheological model in Pujala (2014) is respected. Another important feature implemented in the model is the interfacial tension between dilute sol and seeping water at the expanding front. The results suggest that surface tension effects become important for small apertures and can prevent the sol to expand indefinitely, but the real value of the interfacial tension between sol and seeping water, which is subject to some uncertainties according to Jańczuk et al. (1996), must be further investigated.

Finally, a case representing an extremely erosive scenario with deionized water and high flowrate (test 3 of Schatz et al. 2013) has been simulated with several flow formulations and several permeability models. In first place, the Brinkman equations with the Kozeny-Carman permeability model have been solved, obtaining similar results to those of Neretnieks et al. (2017), i.e. an underestimation of the eroded mass. On the other hand, the same equations with the viscosity-scaled permeability used by Moreno et al. (2010) considerable overestimate the smectite erosion. This proves the importance of solving the flow and transport equations in the compacted bentonite region as well as the presence of the viscous shear term. A similar outcome has been obtained with the Stokes equations, which have been used to evaluate the role of the Darcian term. Therefore, instead of resorting to a two-region model, the previous flow equations with a radial force term accounting for swelling pressure is proposed for reinforcing expansion in front of erosion (Section 4.3.2).

In regard to the solute transport in the buffer under the effect of glacial water, the two simulated approaches, Fickian diffusion with restricted free porosity and the Donnan approach (Birgersson and Karnland 2009), provide upper and lower bounds for the time span before the water surrounding the bentonite buffer reaches CCC. The diffusion through free porosity without the effect of negative surface charge leads to complete leaching, but still, it takes some time to dissolve the plume generated around the bentonite – water interface; from several hundred up to 3 000 years after the arrival of the glacial front, depending on the available porosity and the glacial water flow rate. The scenario of full charge retention represented by the Donnan model yields a more optimistic prediction/estimation of

the leaching rate. In this case, the scenario with standard flow rate according to SKB (2006) reaches CCC after 7 000 years, which still can be considered a relatively pessimistic result because neither accessory minerals nor extruded clay at the interface have been included in the model.

8.2 Remaining uncertainties

The work presented here is a first attempt to extend and improve Neretnieks' model based on physical principles. There are still crucial aspects and uncertainties regarding bentonite integrity that should be further studied. As stated in Chapter 4, a more accurate derivation of the convective term in the smectite expansion equation accounting for wall friction and shear resistance would require: (1) the calculation of the real strain rate with the flow equations and (2) the complete implementation of a non-Newtonian rheological model for the whole range of smectite concentrations.

In regard to erosion, the evaluation of alternative permeability models and the effect of swelling pressure in the Stokes / Brinkman flow equations must still be assessed for a better understanding of the balance between expansion and erosion. Moreover, the presence of a controlled seeping water flow will also reduce the uncertainties regarding water chemistry that affect closed stagnant systems.

Flocculation and gravity effects are also sources of uncertainty (Neretnieks et al. 2017), as well as the role of accessory mineral particles in the clogging of rock fractures (Richards 2010). In the first case, the non-Newtonian behaviour of bentonite sol might become relevant below CCC, where bentonite is more prone to decompose in flocs. Although water chemistry might be the triggering factor, one theory is that high swelling pressure gradients might lead to a local harsh reduction of viscosity due to high strain rates, in turn leading to an early detachment of flocs during expansion. This phenomenon is the base of the model presented by Sato et al. (2004).

Finally, regarding solute transport models in compacted bentonite, two different models are considered in this work, both without the impact of chemical reactions on solute concentrations and porosity distributions. Thus, the time estimated to reach CCC around the buffer should be considered as a first approximation.

References

SKB's (Svensk Kärnbränslehantering AB) publications can be found at www.skb.com/publications.

Adachi Y, Nakaishi K, Tamaki M, 1998. Viscosity of dilute suspension of sodium montmorillonite in an electrostatically stable condition. Journal of Colloid and Interface Science 198, 100–105.

Ahn J, Chambré P L, Verbeke J, 1999. Numerical simulation of bentonite extrusion through a narrow planar space. MRS Online Proceedings Library 608. doi:10.1557/PROC-608-185

Alonso U, Missana T, García Gutiérrez M, Morejón J, Mingarro M, Fernández A, 2019. CIEMAT studies within POSKBAR project. Bentonite expansion, sedimentation and erosion in artificial fractures. SKB TR-19-08, Svensk Kärnbränslehantering AB.

Appelo C A J, 2013. A review of porosity and diffusion in bentonite. Posiva Working Report 2013-29, Posiva Oy, Finland.

Arcos D, Grandia F, Domènech C, 2006. Geochemical evolution of the near-field of a KBS-3 repository. SKB TR-06-16, Svensk Kärnbränslehantering AB.

Badia S, Codina R, 2009. Unified stabilized finite element formulations for the Stokes and the Darcy problems. SIAM Journal on Numerical Analysis 47, 1971–2000.

Birgersson M, Karnland O, 2009. Ion equilibrium between montmorillonite interlayer space and external solution – Consequences for diffusional transport. Geochimica et Cosmochimica Acta 73, 1908–1923.

Birgersson M, Börgesson L, Hedström M, Karnland O, Nilsson U, 2009. Bentonite erosion. Final report. SKB TR-09-34, Svensk Kärnbränslehantering AB.

Börgesson L, Johannesson L-E, Sandén T, Hernelind J, 1995. Modelling of the physical behaviour of water saturated clay barriers. Laboratory tests, material models and finite element application. SKB TR 95-20, Svensk Kärnbränslehantering AB.

Börgesson L, Hedström M, Birgesson M, Karnland O, 2018. Bentonite swelling into fractures at conditions above the critical coagulation concentration. SKB TR-17-11, Svensk Kärnbränslehantering AB.

Borrelli R A, Ahn J, 2008. Numerical modeling of bentonite extrusion and radionuclide migration in a saturated planar fracture. Physics and Chemistry of the Earth, Parts A/B/C 33, S131–S141.

Bourg I C, Bourg A C M, Sposito G, 2003. Modeling diffusion and adsorption in compacted bentonite: a critical review. Journal of Contaminant Hydrology 61, 293–302.

Bradbury M H, Baeyens B, 2003. Porewater chemistry in compacted re-saturated MX-80 bentonite. Journal of Contaminant Hydrology 61, 329–338.

Bruno J, Duro L, 1999. Processes and features affecting the near-field hydrochemistry. Groundwater – bentonite interaction. SKB TR-99-29, Svensk Kärnbränslehantering AB.

Codina R, Baiges J, 2011. Finite element approximation of transmission conditions in fluids and solids introducing boundary subgrid scales. International Journal for Numerical Methods in Engineering 87, 386–411.

COMSOL, 2018. COMSOL Multiphysics® v. 5.4. COMSOL AB, Sweden.

Cronstrand P, 2016. Long-term performance of the bentonite barrier in the SFR silo. SKB TR-15-08, Svensk Kärnbränslehantering AB.

Gens A, 2010. Soil–environment interactions in geotechnical engineering. Géotechnique 60, 3–74.

Girifalco L A, Good R J, 1957. A theory for the estimation of surface and interfacial energies. I. Derivation and application to interfacial tension. The Journal of Physical Chemistry 61, 904–909.

Höglund L O, 2014. The impact of concrete degradation on the BMA barrier functions. SKB R-13-40, Svensk Kärnbränslehantering AB.

Idiart A, Coene A, 2019. Modelling diffusion through compacted bentonite in the BHA vault. Report for the safety evaluation SE-SFL. SKB R-19-10, Svensk kärnbränslehantering AB.

Islam M N, Bunger A P, Huerta N, Dilmore R, 2019. Bentonite extrusion into near-borehole fracture. Geosciences 9, 495.

Jańczuk B, Bruque J M, González-Martín M L, del Pozo J M, Zdziennicka A, Quintana-Gragera F, 1996. The usefulness of the equation of state for interfacial tensions estimation in some liquid–liquid and solid–liquid systems. Journal of Colloid And Interface Science 181, 108–117.

Juntunen M, Stenberg R, 2009. Nitsche's method for general boundary conditions. Mathematics of Computation 78, 1353–1374.

Kanno T, Iwata Y, Sugino H, 2001. Modelling of bentonite swelling as solid particle diffusion. In Adachi K, Fukue M (eds). Clay science for engineering. Boca Raton, FL: CRC Press, 561–570.

Karnland O, Muurinen A, Karlsson F, 2005. Bentonite swelling pressure in NaCl solutions. Experimentally determined data and model calculations. In Alonso E E, Ledesma A (eds). Advances in understanding engineered clay barriers: Proceedings of the International Symposium on Large Scale Field Tests in Granite, Sitges, Barcelona, 12–14 November 2003. London: Taylor & Francis, 241–256.

Laviña M, Idiart A, Molinero J, Casas G, 2018. POSKBAR project. Development, testing and application of alternative models for bentonite expansion and erosion. SKB TR-17-13, Svensk Kärnbränslehantering AB.

Liu L, Moreno L, Neretnieks I, 2009. A dynamic force balance model for colloidal expansion and its DLVO-based application. Langmuir 25, 679–687.

Moreno L, Neretnieks I, Liu L, 2010. Modelling of erosion of bentonite gel by gel/sol flow. SKB TR-10-64, Svensk Kärnbränslehantering AB.

Muurinen A, Lehikoinen J, 1999. Porewater chemistry in compacted bentonite. Posiva 99-20, Posiva Oy, Finland.

Muurinen A, Karnland O, Lehikoinen J, 2007. Effect of homogenization on the micro-structure and exclusion of chloride in compacted bentonite. Physics and Chemistry of the Earth, Parts A/B/C 32, 485–490.

Neretnieks I, 1986. Stationary transport of dissolved species in the backfill surrounding a waste canister in fissured rock: Some simple analytical solutions. Nuclear Technology 72, 194–200.

Neretnieks I, Moreno L, 2018a. Revisiting bentonite erosion understanding and modelling based on the BELBaR project findings. SKB TR-17-12, Svensk Kärnbränslehantering AB.

Neretnieks I, Moreno L, 2018b. Some mechanisms that influence bentonite erosion in a KBS-3 repository – an exploratory study. SKB TR-18-13, Svensk Kärnbränslehantering AB.

Neretnieks I, Liu L, Moreno L, 2009. Mechanisms and models for bentonite erosion. SKB TR-09-35, Svensk Kärnbränslehantering AB.

Neretnieks I, Liu L, Moreno L, 2010. Mass transfer between waste canister and water seeping in rock fractures. Revisiting the Q-equivalent model. SKB TR-10-42, Svensk Kärnbränslehantering AB.

Neretnieks I, Moreno L, Liu L, 2017. Clay erosion – impact of flocculation and gravitation. SKB TR-16-11, Svensk Kärnbränslehantering AB.

Parkhurst D L, Appelo C A J, 2013. Description of input and examples for PHREEQC version 3 – A computer program for speciation, batch-reaction, one-dimensional transport, and inverse geochemical calculations. Techniques and Methods 6–A43, U.S. Geological Survey, Denver, Colorado.

Pujala R K, 2014. Dispersion stability, microstructure and phase transition of anisotropic nanodiscs. Cham, Switzerland: Springer International Publishing.

Richards T, 2010. Particle clogging in porous media. Filtration of a smectite solution. SKB TR-10-22, Svensk Kärnbränslehantering AB.

Sato D, Kobayashi M, Adachi Y, 2004. Effect of floc structure on the rate of shear coagulation. Journal of Colloid and Interface Science 272, 345–351.

Sawada A, Uchida M, Shimo M, Yamamoto H, Takahara H, Doe T, 2001. Anisotropy, reversibility and scale dependence of transport properties in single fracture and fractured zone – Nonsorbing tracer experiment at the Kamaishi mine. In First TRUE Stage – Transport of solutes in an interpreted single fracture. Proceedings from the 4th International Seminar Äspö, September 9–11, 2000. SKB TR-01-24, Svensk Kärnbränslehantering AB, 151–164.

Schatz T, Kanerva N, Martikainen J, Sane P, Olin M, Seppälä A, Koskinen K, 2013. Buffer erosion in dilute groundwater. Posiva 2012-44, Posiva Oy, Finland.

Schramm L L, Hepler L G, 1994. Surface and interfacial tensions of aqueous dispersions of charged colloidal (clay) particles. Canadian Journal of Chemistry 72, 1915–1920.

Sena C, Salas J, Arcos D, 2010. Aspects of geochemical evolution of the SKB near field in the frame of SR-Site. SKB TR-10-59, Svensk Kärnbränslehantering AB.

SKB, 2006. Long-term safety for KBS-3 repositories at Forsmark and Laxemar – a first evaluation. Main report of the SR-Can project. SKB TR-06-09, Svensk Kärnbränslehantering AB.

SKB, 2010. Data report for the safety assessment SR-Site. SKB TR-10-52, Svensk Kärnbränslehantering AB.

SKB, 2011. Long-term safety for the final repository for spent nuclear fuel at Forsmark. Main report of the SR-Site project. SKB TR-11-01. Svensk Kärnbränslehantering AB.

Vowell S, 2009. Microfluidics: the effects of surface tension. Available at: http://citeseerx.ist.psu.edu/viewdoc/download?doi=10.1.1.509.7902&rep=rep1&type=pdf

Wersin P, 2003. Geochemical modelling of bentonite porewater in high-level waste repositories. Journal of Contaminant Hydrology 61, 405– 422.

Wersin P, Curti E, Appelo C A J, 2004. Modelling bentonite–water interactions at high solid/liquid ratios: swelling and diffuse double layer effects. Applied Clay Science 26, 249–257.

Åkesson M, Börgesson L, Kristensson O, 2010. SR-Site Data report. THM modelling of buffer, backfill and other system components. SKB TR-10-44, Svensk Kärnbränslehantering AB.

Appendix A

The equations of Neretnieks' model corresponding to the derivation of the smectite diffusion coefficient (Liu et al. 2009), which have been implemented in COMSOL, are presented below:

$$\partial_t \varphi = -\vec{u}\nabla\varphi + \nabla \cdot (D_F \nabla\varphi)$$

$$D_F = \frac{\chi(1-\varphi)^{1.6}}{f}$$

$$h = \left(\frac{\varphi_{max}}{\varphi} - 1\right)\delta_p$$

$$f = \left[6\pi\eta_w r_{eq} + V_p k_0 \tau^2 a_p^2 \eta_w \frac{\varphi}{(1-\varphi)^2}\right]$$

$$\chi = k_B T + \left(h + \delta_p\right)^2 \left(\frac{\partial F_A}{\partial h} - \frac{\partial F_R}{\partial h}\right)$$

$$\frac{\partial F_A}{\partial h} = -\frac{A_H S_p}{2\pi}\left[h^{-4} - 2\left(h + \delta_p\right)^{-4} + \left(h + 2\delta_p\right)^{-4}\right]$$

$$\frac{\partial F_R}{\partial h} = -4\kappa c R T S_p \tanh y^m \left[\cosh y_\infty^m \sinh\left(\frac{y_\infty^m}{2}\right) + \frac{1}{\kappa h}\sinh y_\infty^h + \frac{2}{(\kappa h)^2}\sinh\left(\frac{y_\infty^h}{2}\right)\right]$$

$$y^m = \operatorname{asinh}\left[2\sinh y_\infty^m + \frac{4}{\kappa h}\sinh\left(\frac{y_\infty^h}{2}\right)\right]$$

$$y_\infty^m = 4\,\operatorname{atanh}\left[\tanh\left(\frac{y_\infty^0}{4}\right)\exp\left(-\frac{\kappa h}{2}\right)\right]$$

$$y_\infty^h = 4\,\operatorname{atanh}\left[\tanh\left(\frac{y_\infty^0}{4}\right)\exp(-\kappa h)\right]$$

$$\kappa = \left(\frac{2F^2 c z^2}{\varepsilon_0 \varepsilon_r R T}\right)^{1/2}$$

$$y_\infty^0 = 2\,\operatorname{asinh}\left(\frac{S_0}{2}\right)$$

$$s_0 = \frac{zF\sigma^0}{\varepsilon_0 \varepsilon_r \kappa R T}$$

For the simulation of test 3 (Schatz et al. 2013) involving bentonite erosion, the gel-sol viscosity correlation presented by Adachi et al. (1998) has also been implemented:

$$\eta_{rel} = 1 + 1.022\varphi_{cov} + 1.358\varphi_{cov}^3$$

$$\varphi_{cov} = \frac{2}{3}\frac{(D_P + 2m\kappa^{-1})^3}{D_p^2 \delta_p}$$

Notation	Property	Value and/or unit
k_B	Boltzmann's constant	1.380×10^{-23} J/K
r_{eq}	Equivalent radius of non-spherical particles	63.66 nm
F	Faraday's constant	96 485 C/mol
m	Fitting parameter in co-volume fraction	1
R	Gas constant	8.314 J/(K mol)
A_H	Hamaker constant	$2.5k_BT$
$k_0\tau^2$	Kozeny's constant	5, 13
φ_{max}	Maximum volume fraction of smectite	1
ε_0	Permittivity of vacuum	8.854×10^{-12} F/m
ε_r	Relative permittivity of water	78.54
D_P	Smectite particle diameter	200 nm
δ_p	Smectite particle thickness	1 nm
a_p	Specific surface area per unit volume of particles	$2/\delta_p$ m^2/m^3
S_p	Surface area of smectite particle	3.1415×10^{-14} m^2
σ^0	Surface charge of particles	−0.131 C/m^2
T	Temperature	298.15 K
z	Valence of counterion	1
η_w	Viscosity of water	1.002×10^{-3} N s/m^2
φ	Volume fraction of smectite – variable	-
V_p	Volume of the smectite particles	3.1415×10^{-23} m^3

Arkitektkopia AB, Bromma, 2020

SKB is responsible for managing spent nuclear fuel and radioactive waste produced by the Swedish nuclear power plants such that man and the environment are protected in the near and distant future.

skb.se